POLITECNICO DI TORINO

Master's degree programme in Civil Engineering

Politecnico di Torino

Master Thesis

Theoretical Investigation of Multiple Pounding in Curved Bridges due to Vertical Ground Motion

Supervisors

Prof. Gian Paolo Cimellaro

Dr. Alessandro Cardoni

Candidate

Zukhuriddin Abdubokiev

A.Y. 2023/2024

Index

I. **Chapter 1: Introduction**

II. **Chapter 2:**

2.1 Continuous Curved Bridges

2.1.1 Curved Bridges: Structure and Significance

2.1.2 Geometry and Behavior

2.1.3 Problems Associated with Bridge Curvature.

2.1.3.1 Bearing Unseating

2.1.3.2 Complex Dynamic Behavior

2.1.3.3 Torsional Problem

2.1.3.4 Pounding Effect

2.2 Curved Bridges: Theory and analysis

2.2.1 Global Structural Analysis of Curved Bridge.

2.2.2 System of Coordinates.

2.2.3 Fundamental DFE for Stress Resultants

2.2.4 Fundamental DFE for Displacements

2.2.5 Solution for Moment

2.2.6 Solution for Torsion using Approximate Method

2.2.7 Solution for Torsion through Statics

2.2.8 Dynamic of a Curved Beam

2.2.8.1 Governing Equation of Motion of Curved Beam

2.2.8.2 Frequency Determination for Curved Beam

III. **Chapter 3:**

3.1 Case Study

3.1.1 Overview

3.1.2 Static Solution

3.1.2.1 Vertical Quasi-static Displacement for In-contact Phase

3.1.2.2 Vertical Quasi-static Displacement for Out-of-contact Phase

3.1.3 Dynamic Solution

3.1.3.1 Vertical Dynamic Displacement for In-contact Phase

3.1.3.2 Vertical Dynamic Displacement for Out-of-contact Phase

3.2 Numerical Results

3.2.1 Bridge Parameters

3.2.2 Convergence of Analysis Outcome

3.2.3 Wave propagation across the beam induced by vertical ground motion
3.2.4 Multiple Pounding Phenomena
3.2.5 Mode Shapes
3.2.6 Response of the bridge under uniform seismic excitation

IV. Chapter 4: Conclusion

V. Appendix

Introduction

Design and analysis in the bridge structure, especially under seismic action, are one of the most critical aspects within civil engineering. Curved bridges are normally adopted because of the esthetic point of view in landscape designs along with the economy of space. In seismic impacts, this geometrical nonlinearity creates additional challenges. The above thesis entitled "Theoretical Investigation of Pounding Effect Generated in Curved Bridges" provides information about the dynamic responses of such kind of structures to seismic forces, putting a spotlight on this phenomenon.

Pounding effect occurs when oscillating bridge segments collide during earthquakes, potentially causing significant damage both on girder and isolation system. The risk of such impacts is prominent in horizontally curved bridges due to their varying radii and altered dynamic properties. This study systematically investigates how different curvature radii influence the pounding or contact forces at the critical girder-pier interfaces due to the vertical component of seismic events, providing insights that are crucial for the design and retrofitting of safer bridges and viaducts.

To achieve a comprehensive understanding, this research employs a dual approach combining theoretical analytical methods with sophisticated finite element analysis. This methodology allows for the precise modeling of seismic interactions within curved bridge structures under various vertical seismic excitations. By changing the seismic input periods to match and deviate from the natural periods of the bridge in both in-contact and out-of-contact phases, the study points out the influence of period matching on the intensity and magnitude of pounding phenomena.

The present work contributes to the number of fields, significantly earthquake and bridge engineering by elucidating the impact of structural curvature on the dynamic responses of bridges. The findings are intended to guide the development of advanced design strategies that enhance the structural resilience and safety of in-plane curved bridges in earthquake-prone areas. Through this detailed exploration, the research aims to support the engineering community in creating bridge designs that not only meet technical and functional requirements but also withstand the challenges posed by seismic excitations.

Chapter 2

2.1 Continuous Curved Brdiges

2.1.1 Curved Bridges: Structure and Significance

Bridges with curved alignment were once uncommon, but nowadays, the majority of straight bridges have become curved due to various factors such as site constraints, architectural considerations, traffic volume, and changes in speed limits. The curved bridge design is widely recognized for its effectiveness, stability, functionality, economy, and aesthetics. These bridges are often selected to have a circular plan with transition curves.

Figure 1.1. Curved I-girder viaduct

Analyzing bridges curved in the plan is more complex than analyzing straight bridges because they are subjected to a combination of bending and torsion induced by the curvature of the girders. Therefore, when designing a curved bridge, it's crucial to choose a section with high torsional stiffness to ensure efficiency. However, in small curvature bridges, the effect of the curve angle on bending moments (BM), shear forces (SF), torsional moments (TM), and vertical deflections (VD) may be negligible if it remains within acceptable limits.(Agarwal et al.)

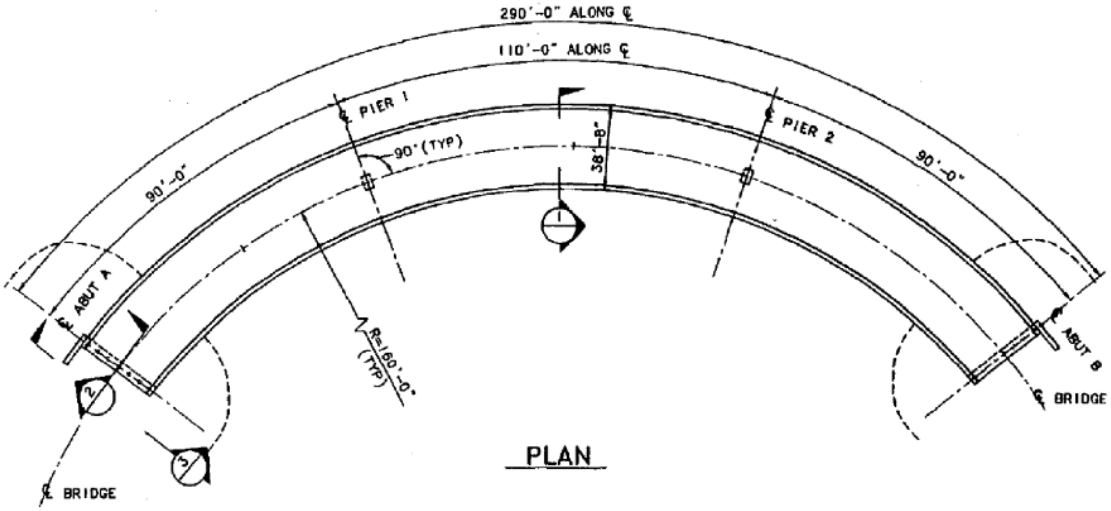

Figure 1.2. Box-girder curved bridge

One of the most common techniques for analyzing and designing curved bridges is to treat them as if they were straight, with well-defined limitations. In curved bridges, torsion is induced, affecting the bridge's response in terms of flexural behavior, shear, and torsion. It twists the bridge cross-section and generates uneven stresses in the flange. Thanks to the accessibility of high-capacity computational systems, the analysis and design of curved bridges with greater curvature have become more manageable.

So far, many studies were conducted on curved bridges and some latest of them are included in this thesis. Gupta et al. (2019a, b) performed the static analysis of RC curved box-girder bridge using SAP2000 software and determined that the effect of curvature angle under the 12° is not significant on forces and deflection. Agarwal et al. (2019) investigated the maximum bending moment and shear force in a single-cell skewed box-girder bridge by FEM. Tamaddon (2020) studied the effect of curvature angle of curved RC box-girder continuous bridges on their transient response and vertical pounding subjected to near-source earthquake. Agarwal et al. (2020a, b) examined the behavior of RC skew box-girder bridge subjected to Indian loadings using CsiBridge. Gupta (2022) illustrated seismic response of horizontally curved bridges in combination with skewed abutments. Mairone et al. (2022a,b) decoupled the coupling between bending and torsion that arises in curved bridges by solving differential equations and presented a case study on a horizontally curved steel box-girder bridge located in North of Italy. Guan et al. (2023) introduced the method to identify the critical seismic input for curved bridges.

2.1.2 Geometry and Behaviour

The use of horizontally curved steel girders in highway bridges has seen remarkable developments over the past several decades. Initially, when curved bridge superstructures were introduced, they typically consisted of a series of straight girder chords. In the early years of modern bridge design, engineers hesitated to employ curved girders due to the mathematical complexities associated with their design.(Mairone et al.)

Bridges with complex geometries or structures featuring curvilinear axes with variable radii are sometimes necessary for optimizing road paths and minimizing material usage. To address the complex stress redistribution and torque, the superstructure of curvilinear viaducts can be characterized by decks with specific cross-sectional geometries, including:

- Box decks with a single cell, composed of composite steel-concrete, prestressing steel, or steel materials (Figure 1(a)).

- Box beams interconnected with a slab (Figure 1(b)).
- Multicellular box decks in steel, prestressed concrete, or composite systems (Figure 1(c)).
- Decks with I-section beams in reinforced or prestressed concrete.

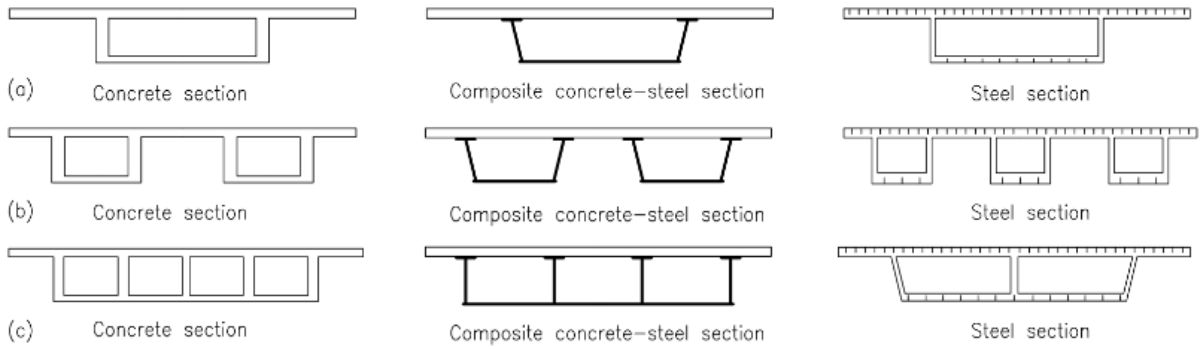

Figure 1.3. Types of box section: (a) Single cell; (b) Interconnected single-cell; (c) Multicellular;

The use of closed sections has proven to be an efficient structural solution for bridges and flyovers 6. These closed sections offer high torsional stiffness, efficient distribution of eccentric variable traffic loads among the cores of the box girder, and benefits in terms of maintainability, economy, and aesthetics.

However, curvilinear bridge decks always exhibit torsional deformation under vertical loads, resulting from an eccentricity between applied loads and support reactions. Consequently, an interaction between bending and torsion moments occurs along the spans. While finite element models facilitate this analysis, analytical calculations often treat bridges with curvilinear layouts as horizontally curved structures.

According to the type of cross-section, the torsional behavior of bridge decks can be described by two main categories:

- Open cross-sections: These are often obtained either by using two main beams (twin girder) or several main beams (multi-girder). Open cross-sections resist non-uniform (warping) torsional actions and provide limited torsional rigidity.
- Closed cross-sections: These may comprise a box that is entirely made of steel, a steel U-shaped section, or a twin girder section closed by lower plan bracing. Essentially, closed cross-sections resist uniform (St-Venant) torsion and deform very little. These systems are advantageous for bridges subjected to significant torsion, such as curved bridges or bridges with substantial cantilevers to the slab.

In the present thesis, we discuss different analytical and numerical approaches that can be used to design horizontally curved girders, focusing on a case study of a steel-box girder bridge. Here are the key points:

1. Analytical Approach: Originally used by designers, this approach is strongly simplified and conservative in terms of torque action computations.
2. Improved Analytical Evaluation: We propose an improved analytical evaluation of the torque action based on a more realistic representation of boundary conditions.
3. Finite Element Method Calculations: We present finite element method calculations with varying levels of detail regarding the geometrical description of the bridge.

The main aim is to highlight the advantages and disadvantages of different approaches available for designing such complex structures, including analytical formulations and numerical models. The case study involves a simple bridge with only three spans, allowing us to analyze different load and boundary conditions that significantly impact the interplay between bending and torque actions.

2.1.3 Specific problems related to curved bridges.

2.1.3.1 Bearing unseating

Multi-span bridges on connecting roads at highway junctions are usually constructed of reinforced concrete or prestressed concrete. These are usually structures with beams, beams or hollow girder sections. Despite many years of experience in planning such structures, unfortunately there are still cases in which negative events and problems occur that were not foreseen by the planners and contractors. This is especially true for prestressed structures that cannot be determined statically. The most common problems are separation of the head plate from the outermost bearing and its overloading, excessive mutual displacement of the bearing plates in plan, changes in the shape of the superstructure, and changes in the inclination of the superstructure. cross beam. A section also related to reaching the permissible rotation angle of the bearing.

Separation of the head plate on the outermost bearing is related to the uneven distribution of loads on pairs of bearings on the same support. This is because there is a significantly larger torsional moment than in a simple structure. In most cases this involves bearings on the abutment, and for obvious reasons the reaction force is often less than half of the reaction force on the intermediate support. Dead load distribution in the presence of strong curvature is the reason why there is significantly more material on the outside of the connecting road. As a result, the reaction force at the bottom bracket is lower, and preload effects and unfavorable payload distribution can reduce the reaction force and cause the top plate to rise (Figure 4).

Typical bridge bearings are not designed for this type of work. A minimum amount of pressure is required so that the bearing performs its function and does not cause damage or accelerated wear. Overloading of the inner bearing is usually accompanied by overloading of the adjacent outer bearing. If not anticipated by the designer, unexpectedly exceeding the load capacity can cause permanent damage to the support structure, requiring replacement (Figure 6)

Proper support of a structure requires bearings that provide the maximum possible flexibility with respect to deformation of the superstructure while meeting the general stability conditions. Structures with large curvatures are very difficult to avoid deforming. Among the many ways to support the field on bearings, there are two methods that are most commonly called: tangent and radius.(Klikowicz et al.)

The first method (tangential) is to align the deformation due to thermal effects along the beam axis. Such an arrangement typically introduces additional stresses in areas where the structure is not deformed.

The second method (radial section) minimizes the additional internal forces caused by additional members in the plan and maximizes the freedom of displacement. The deformation is directed along the line defined by the section from the specified direction bearing to the fixed bearing.

Depending on the bearing, the internal forces of every action have different values. Thermal and rheological effects and compression of the strongly curved multi-span superstructure result in floor plan deviations and deformations. The upper plates of plain bearings move relative to each other. A lack of detailed analysis of these interactions during the design stage may result in bearings having too little freedom of movement, which could lead to excessive slippage or axle carrier drop in emergency situations. It can appear during operation (Figure 5).

Fig.1.4. Detachment of bearing top's plate

Fig.1.5. Excessive displacement of bearing plate

Fig.1.6. The effect of bearing overload

2.1.3.2 Complex dynamic response.

In general, box girder bridges are used when larger spans and wider bridge decks arise. They have high strength and greater torsional and bending stiffness. The straight bridge deck is supported orthogonally to traffic. But due to some reasons, such as site conditions and land acquisition issues, the axis of the bridge may not be perpendicular to the piers supporting the ground and such bridges are said to be skewed as shown in Figure 1a. Many straight bridges can also be curved in plan (Figure 1b) due to speed variations, high traffic volumes, site constraints, and alignment configurations. The combination of two different bridges mentioned above results in an obliquely curved bridge, as shown in Figure 1c. The response of these types of bridges cannot be measured directly by adding the individual effects of asymmetry and curvature. So, it is necessary to combine the effects of skewness and curvature at the analysis stage itself to assess the structural behaviour of skew-curved bridges. The free vibration analysis is very important to determine the structure's response to check whether the deck's natural frequency is away from excitation frequencies. The free vibration occurs naturally, with no energy being

added to the vibrating system. The vibration starts with some energy input but dies away with time as the energy is dissipated. The natural frequencies and vibration modes depend upon the whole system, i.e., road characteristics, the material used, cross-sectional properties, etc. Because vibration is proportional to the mass of the system, steel and prestressed concrete bridges are more susceptible to vibration than concrete bridges.

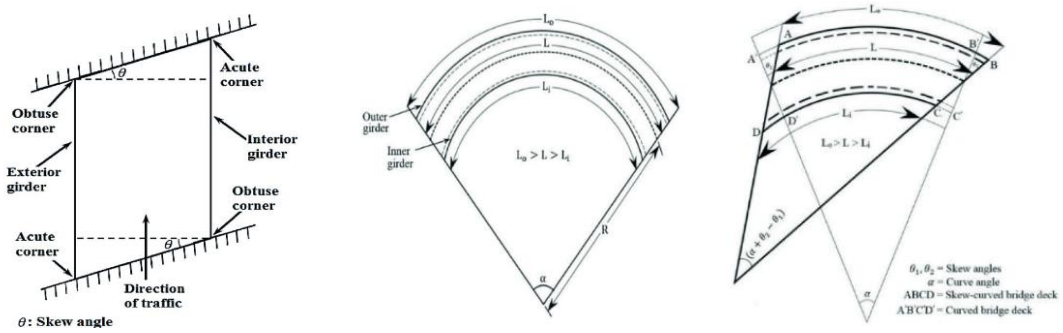

Fig 1.7. a. Skew (left), b. Curved (middle) c. Skew-curved (right) box girder bridges.

Several commercial software programs based on the finite element method (FEM) are available. For bridges, which are large structures or similar structures, FEM-based software can be used to evaluate the natural frequencies, regardless of the size and complexity of such structures.

In study of (Gupta and Sandhu), skew-curved bridges have been studied for their seismic behavior under both free and forced vibrations. Using 3-D bridge models in CSiBridge, we varied the skew angle (θ) from 0° to 60° at 15° intervals and the curvature angle (β) from 0° to 90° at 30° intervals. The detailed finite element analysis assessed how these bridges respond to seismic forces when subjected to both free and forced vibrations.

Modal analysis results reveal that regardless of skewness and curvature, the in-plane vibrational mode is the fundamental mode of bridge vibration, followed by longitudinal and out-of-plane modes. For the first in-plane vibrational mode the time-period increases with the skew angle and vice versa, it decreases with the degree of curvature. The mode participation factor becomes higher for skew-curved bridges when introducing greater angles than the bridge's original configuration. Generally, the mode participation factor of the third out-of-plane vibrational mode decreases with increasing skew and curvature angles. However, for higher curvature angles (i.e., β = 90°), introducing skew angles leads to an increased mode participation factor for this mode.

Seismic behavior of skew-curved bridges has been thoroughly investigated under forced vibrations. The analysis involved response spectrum analysis using design response spectra from AASHTO 2007. From that analysis, it was found that, under longitudinal seismic excitations, the in-plane bending moment is significantly higher for curved and skew-curved bridge configurations compared to skew bridges. As the curvature angle increases, the longitudinal torsion and out-of-plane bending moment also increase. However, with an increase in skewness, longitudinal torsion increases while out-of-plane bending moment decreases. For straight bridge configurations, very little out-of-plane bending moment is noticed under transverse excitations. Introducing curvature increases the demand for out-of-plane bending moment, and this effect becomes more pronounced with greater curvature angles. Under transverse excitations, all the principal moments decrease as the curvature of the bridge deck increases. The in-plane bending moment under transverse seismic excitations experiences very high demand. Changes in bridge configuration cause only a slight variation in all the principal moments under vertical seismic excitations.

Above research helps to understand that, depending on skew and curvature angle, the bridge exhibits different type of behavior compared to straight ones. Consequently, a bridge may undergo unpredicted way of loadings that have to be taken into account through rigorous analysis.

2.1.3.3 Torsional Problems

As it was mentioned previously, due to the particular geometry of a curved bridges, torsion interacts with moment that can't be said about straight ones. In curved bridges torsion is induced by vertical loads, the loads that is symmetrical about longitudinal axis of the structure. Bending and torsion are coupled, and their relationship depends on mainly:

- Raduis of curvature
- Bending to torsional stiffness ratio *EI/GK*
- Boundry conditions

The problem be solved using either by using approximate method (Reis and Pedro) or by classical curved beam theory which is based on balance equations between internal forces and applied external loads that can be established through statics by considering an element of a curved girder with an infinitesimal length.

2.1.3.4 Pounding effect

Although the effect of pounding is as a one of above listed problems in curved bridges, it might be the main cause of the other type of failures that will follow. For instance, due to the high vertical seismic forces, the deck can be separated from the pier which leads to unseating. Moreover, in combination with horizontal components of earthquake, the bridge is susceptible to global damage when the deck may collapse after separation. Therefore, the close attention was given to this phenomenon in this thesis. Pounding on curved bridge is more significantly influenced by the change in parameters, such as excitation conditions and expansion joint gap size. There are several poundings:

- Span to span
- Abutment to span
- Pier to span

After the strong earthquake of 1971 in San Fernando, (Jennings and Wood) where a number of curved bridges were destroyed, many authors started to study pounding phenomena caused by horizontal components of earthquake. (Li et al.) conducted shake table test on a 1/10 scaled curved bridge model to study the influence of adjacent pounding (AP) on excitation conditions and gap size. Author found that the state of excitation waves and pounding force peak values can be greater under the bidirectional excitation than those the unidirectional one. Gap size decrease the pounding frequency, but peak pounding force does not decrease as gap size increase. Bridges are vulnerable to local damage due to seismic pounding between the deck and the abutment at expansion joint and this type of seismic seismic damage is much more serious in short span highway bridges, specifically those with an irregularly shaped deck. Abutment-span pounding was investigated and analytical model was introduced by (Amjadian and Agrawal) to identify the parameters affecting the seismic response quantities of curved bridges. Obtained results were verified by FEM analysis.

Fig 1.8. Curved bridge collapse due to 1971 San Fernando earthquake

Above studies illustrate the behavior of a curved bridges only under horizontal excitations, however, the impact of the pounding due to vertical components of earthquake has been rarely considered. In previous researches, it was shown that the peak motion of the earthquake is characterized by a P wave and vertical component has a lower frequency than a P wave. Moreover, as the source-to-site distance increases, the vertical component dampens faster than horizontal one. Therefore, for better seismic evaluation, a parameter so called vertical to horizontal component acceleration (V/H) ratio was adopted. According to studies based on real events, it was found that V/H ratio is highly dependent on source-to-site focal distance at less than 20 km. Further investigation showed that V/H ratio is larger than one at distance less than 5 km and it is greater than 2/3 at distances between 5-25 km. Another key parameter is the time interval between the instant maximum vertical and horizontal accelerations. Typically, the maximum vertical acceleration occurs slightly earlier than maximum horizontal acceleration, the same can be said about P waves that arrive earlier than S waves since the propagation speed is higher in first case. Thus, pounding due to the vertical component may damage a deck before horizontal component start to vibrate the bridge. With high frequencies and large amplitude, pounding may cause separation of members, collision of bridge components, girder detachment, destruction of rubber bearings and failure of piers.

Due to the irregular geometry and nonuniform mass distribution, curved bridges are more vulnerable to effect of pounding caused by vertical excitations than straight bridges. X. Yin (2015) investigated the pounding force due to the vertical component of earthquake by introducing theoretical approach on continuous beam-spring-rod model subjected to multiple vertical pounding derived by the expansion of transient wave functions in a series of eigenvalues.

2.2 Curved Bridges: Theory and analysis.

2.2.1 Global structural analysis.

To fully understand the statics of curved girder, it is always convenient to consider girder as a beam with generic and unsymmetrical cross-section due to the following main reasons:

- The cross-section of girder bridges has various type of forms and dimensions depending on type of bridges, span length, designation and etc.
- Outer girder experiences higher stresses compared to inner one because of centrifugal force of vehicle that can be accommodated by suitable cants to prevent vehicles sliding outward. Therefore, outer girder requires larger dimensions and needs to be designed to handle increased stresses.

In such cases, the shear center of the cross-section doesn't coincide with the center of gravity as in Fig. 2.1 which leads moment-torsion coupling. This phenomenon is already studied S.P Timashenko for straight beams. On top of that, the center of gravity moves towards the concave side of a beam due to the curvature. Komatsu and Nakai introduced the practical formulae for static equations of curved beam using Vlaslov's thin-walled beam theory in addition to determining frequency equations which is discussed later in details.

2.2.2 System of coordinates.

First, analyzing the general section of curved girder, let's denote shear center, center of figure, the center of gravity and the loading point as S, O_n, G and P respectively. These points lay on the circumferences of the circles with radius R_s, R_o, R_G and R_P away from center of curvature $O - O$ as in Fig.2.1

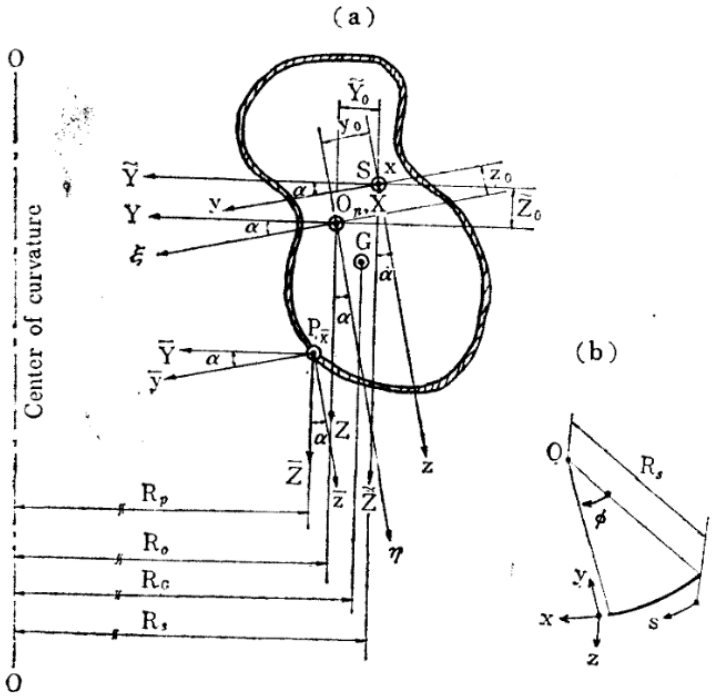

Fig 2.1. System of coordinates of curved bridge girder.

Then, we consider two kinds of coordinate systems: right-hand rectangular coordinates (X, Y, Z) along longitudinal axis through the center O_n, rectangular coordinates (ξ, η) parallel to both principal axes through the same point O_n inclined at an angle α. Orthogonal system of coordinates (x, y, z) and $(x, \hat{Y}, \hat{Z})$ through shear center S are parallel to the axes O_nX, $O_n\xi$, $O_n\eta$ and O_nX, O_nY, O_nZ

respectively. A point P on girder surface is selected to represent the location of external force action. Similarly, the pair of orthogonal coordinates $(\bar{x}, \bar{y}, \bar{z})$ and $(\bar{x}, \bar{\mathrm{Y}}, \bar{\mathrm{Z}})$ through the point P are parallel to the axes Sx, Sy, Sz and $SX, S\hat{\mathrm{Y}}, S\hat{\mathrm{Z}}$ respectively. Following relationship can be given between (y, z) and $(\hat{\mathrm{Y}}, \hat{\mathrm{Z}})$:

$$\begin{aligned} y &= \hat{Y}\cos\alpha + \hat{Z}\sin\alpha \\ z &= -\hat{Y}\sin\alpha + \hat{Z}\cos\alpha \end{aligned} \tag{1.1}$$

The same relationships are held between $(\bar{y}, \bar{z})$ and $(\bar{\mathrm{Y}}, \bar{\mathrm{Z}})$. As it was stated previously, circumferential coordinates on shear center can be written as (see Fig.2.1):

$$s = R_S\varphi \tag{1.2}$$

Basic equations are now derived by using curvilinear coordinates:

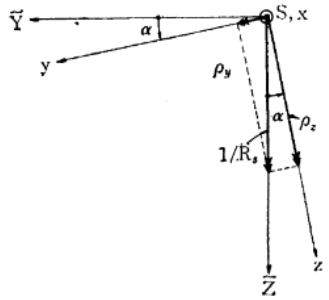

Fig 2.2. Components of curvature

Above figure demonstrates the components of curvature about the axes Sy and Sx, thus:

$$\begin{aligned} \rho_y &= \sin\alpha / R_S \\ \rho_z &= \cos\alpha / R_S \end{aligned} \tag{1.3}$$

2.2.3 Fundamental Differential Equations for Stress Resultants

Let's examine now the equilibrium of stress resultants acting on differential element cut off by two adjacent s and $s + ds$ sections as earlier when we considered the infinitesimal part of curved beam to analyze torsion. Fig.2.3 illustrates internal forces at any cross-section s.

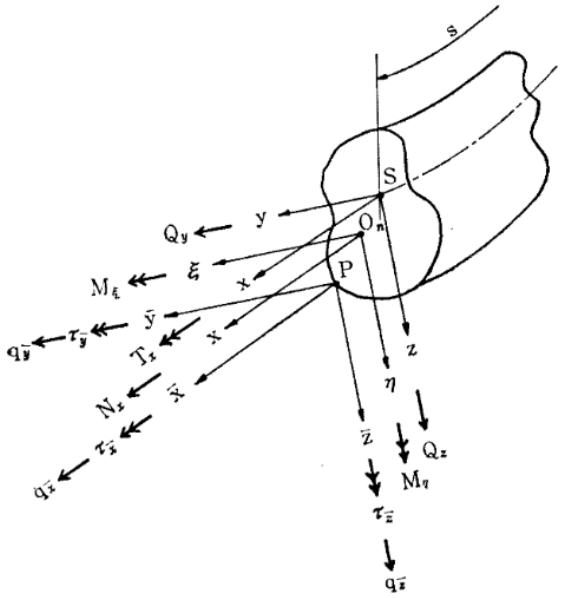

Fig 2.3. Stress Resultants.

N_X is the axial force along O_nX axis, V_y, V_z are shear forces along S_y, S_z axes, T_x is the torsional moment about S_x and M_ξ, M_η are two bending moment about $O_n\xi$, $O_n\eta$ axes. By translating all the forces to the shear center, the following linearized equation can be obtained in the direction of axes x, y and z:

$$\begin{aligned}
&\frac{dN_X}{ds} - \rho_z V_y + \rho_y V_z + \frac{R_P}{R_S} q_{\bar{x}} = 0 \\
&\frac{dQ_y}{ds} + \rho_z N_X + \frac{R_P}{R_S} q_{\bar{y}} = 0 \\
&\frac{dQ_z}{ds} - \rho_y N_X + \frac{R_P}{R_S} q_{\bar{z}} = 0
\end{aligned} \tag{1.4}$$

Since shear and gravity center are not at the same point, it is necessary to take into consideration also moments caused by eccentricity of external torque and stress forces. Moment equilibrium resultants can be given as:

$$\begin{aligned}
&\frac{dT_x}{ds} - \rho_z M_\xi + \rho_y M_\eta - \left(\rho_y y_0 + \rho_z z_0\right) N_X + \frac{R_P}{R_S}\left(\tau_{\bar{x}} - z_P q_{\bar{y}} + y_P q_{\bar{z}}\right) = 0 \\
&\frac{dM_\xi}{ds} + z_o \frac{dN_X}{ds} + \rho_z T_x - Q_z + \frac{R_P}{R_S} \tau_{\bar{y}} = 0 \\
&\frac{dM_\eta}{ds} + y_o \frac{dN_X}{ds} - \rho_z T_x + Q_z + \frac{R_P}{R_S} \tau_{\bar{z}} = 0
\end{aligned} \tag{1.5}$$

Whereas symbols y_o, z_o and y_p, z_p mean coordinates of O_n and P with respect to y, z coordinates. These coordinates have been already provided in Eq.(1.1). In case curved girder is subjected to arbitrary external force, one is able to readily solve Eq.(1.4) for stress resultants N_X, V_y, V_z and substituting those values into Eq.(1.5) it is possible to get stress resultants T_x, M_ξ, M_z.

In actual loading conditions a bridge rarely undergoes force along the axial direction except horizontal components of seismic activity, therefore:

$$q_{\bar{x}} = 0 \tag{1.6}$$

If a transversal load q acts at an angle δ from vertical axis as shown in Fig.2.4, the horizontal and vertical components of q in the directions O_nX and O_nY can be determined:

$$\begin{aligned} q_{\hat{y}} &= q \sin \delta \\ q_{\hat{z}} &= q \cos \delta \end{aligned} \tag{1.7}$$

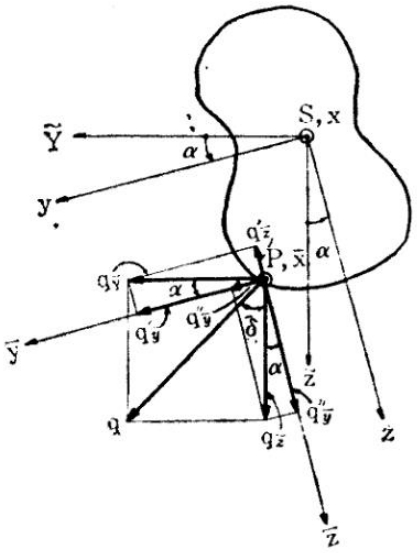

Fig 2.4. Arbitrary force q.

So, in the direction of $\bar{x}$ and $\bar{y}$ components of $q_{\hat{Y}}$ are again rewritten as:

$$\begin{aligned} q_{\bar{y}}' &= q \cos \alpha \sin \delta \\ q_{\bar{z}}' &= -q \sin \alpha \cos \delta \end{aligned} \tag{1.8}$$

and by substituting these into Eq. (1.4) we get differential equation of normal force due to the horizontal component of q:

$$\frac{d^2 N_X}{ds^2} + \frac{N_X}{R_S^2} = -\frac{R_P}{R_S^2} q \sin \delta \tag{1.9}$$

The same procedure can be repeated for $q_{\hat{Z}}$:

$$\begin{aligned} q_{\bar{y}}'' &= q \sin \alpha \cos \delta \\ q_{\bar{z}}'' &= q \cos \alpha \cos \delta \end{aligned} \tag{1.10}$$

The differential equation of normal force due to vertical component of q then becomes:

$$\frac{d^2 N_X}{ds^2} + \frac{N_X}{R_S} = 0 \tag{1.11}$$

Practically, vertical force in most cases is only the dead load while horizontal force can be live load in terms of centrifugal movement of vehicles running along longitudinal curved axis. However, the magnitude of the horizontal force in comparison with the vertical load is so small, that it's effect can be neglected. For this reason, in general δ might be considered as zero:

$$\delta = 0 \tag{1.12}$$

Consequently, the differential equation for normal force reduces to Eq.(1.11), the solution is:

$$N_X = C_1 \sin\varphi + C_2 \cos\varphi \tag{1.13}$$

The boundary condition is as in case of simply supported beam where one end is fixed, and another end is free to move in longitudinal direction. There is no axial force at both $\varphi = 0$ and $\varphi = \Phi$ ends, which means $C_1 = C_2 = 0$. So, we get:

$$N_X = 0 \tag{1.14}$$

In other words, there is no normal force acting at any cross section. Accordingly, the new approximated differential equation is obtained by eliminating axial force from Eq. (1.4) and Eq.(1.5):

$$\begin{aligned}
&\frac{dT_x}{ds} - \rho_z M_\xi + \rho_y M_\eta = -\frac{R_P}{R_S}\left(\tau_{\bar{x}} - z_P q_{\bar{y}} + y_P q_{\bar{z}}\right) \\
&\frac{d^2 M_\xi}{ds^2} + \rho_z^2 M_\xi - \rho_y \rho_z M_\eta = -\frac{R_P}{R_S}\left[q_{\bar{z}} - \rho_z\left(\tau_{\bar{x}} - z_P q_{\bar{y}} + y_P q_{\bar{z}}\right)\right] \\
&\frac{d^2 M_\eta}{ds^2} + \rho_y^2 M_\eta - \rho_y \rho_z M_\xi = \frac{R_P}{R_S}\left[q_{\bar{y}} - \rho_y\left(\tau_{\bar{x}} - z_P q_{\bar{y}} + y_P q_{\bar{z}}\right)\right]
\end{aligned} \tag{1.15}$$

Above equations represent the relation between moments and torsion, previous chapters already contain the solutions for each of them as a function of opening angle so that these parameters are not interdependent.

2.2.4 Fundamental Differential Equations for Displacements

In this chapter we closely analyze the dependency between shear as well as moments and displacements u, v, w in the direction Sx, Sy, Sz axes. Rotation about Sx is denoted by symbol β.

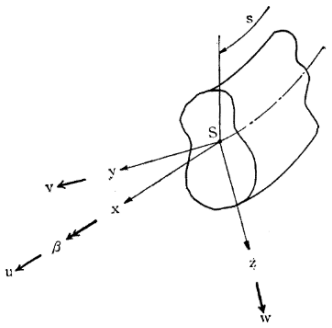

Fig 2.5. Displacements u, v, w and β at shear center S.

These distortions referring to point S will produce additional twisting angle ϑ in the cross-section s and curvature ρ_y', ρ_z' in the cross-section $s + ds$. If the radius of the curvature is constant all over the span, these quantities can be described as below:

$$\rho_y' = \rho_y + \rho_z\beta - \frac{d^2w}{ds^2} + \rho_y\frac{du}{ds}$$
$$\rho_z' = \rho_z - \rho_y\beta + \frac{d^2v}{ds^2} + \rho_z\frac{du}{ds} \tag{1.16}$$
$$\vartheta = \frac{d\beta}{ds} + \rho_y\frac{dv}{ds} + \rho_z\frac{dw}{ds}$$

Next, by integrating ϑ with respect to variable s and assuming rotation matrix as rigid body we obtain the notation θ called as torsional angle:

$$\theta = \beta + \rho_y v + \rho_z w \tag{1.17}$$

On the other hand, the axial strain at shear center can be expressed as follows:

$$\varepsilon_x = \frac{du}{ds} - \rho_z v + \rho_y w \tag{1.18}$$

Knowing the moments and product of inertia $I_{Y,}I_X$ and I_{XY} with respect to axis O_nY and O_nZ, the angle α and principal moments of inertia I_ξ and I_η can be estimated by following formulas:

$$\alpha = \frac{1}{2}\tan^{-1}\left(\frac{2I_{YZ}}{I_Z - I_Y}\right) \tag{1.19}$$

$$I_\xi = \frac{1}{2}\left[I_Y + I_Z + \sqrt{\left(I_Y - I_Z\right)^2 + 4I_{YZ}^2}\right]$$
$$I_\eta = \frac{1}{2}\left[I_Y + I_Z - \sqrt{\left(I_Y - I_Z\right)^2 + 4I_{YZ}^2}\right] \tag{1.20}$$

Taking into account the Eq.(1.6):

$$T_x = G_sJ\frac{d\theta}{ds} - E_sC_w\frac{d^3\theta}{ds^3}$$
$$M_\xi = \frac{R_S}{R_O}E_SI_\xi(\rho_y' - \rho_y) \tag{1.21}$$
$$M_\eta = \frac{R_S}{R_O}E_SI_\eta(\rho_z' - \rho_z)$$

Whereas:

E_s: Young's modulus

G_s: shear modulus of elasticity

J: torsional constant

C_w: warping constant

Torsion consists of two components: left hand side is called St. Venant's torsional moment T_s, another term is T_w is torsional moment due to warping. Wrapping moment is denotes as M_w.

$$T_s = G_s J \frac{d\theta}{ds} \tag{1.22}$$

$$T_w = -E_s C_w \frac{d^3\theta}{ds^3} \tag{1.23}$$

$$M_w = E_s C_w \frac{d^2\theta}{ds^2} \tag{1.24}$$

If we express strain through M_ξ, M_η and M_w, it yields:

$$\varepsilon_x = -\frac{R_o}{R_S}\frac{1}{E_s}\left[\frac{M_\xi}{I_\xi}\eta_s + \frac{M_\eta}{I_\eta}\xi_s\right] + \frac{M_w}{E_s C_w}W_s \tag{1.25}$$

ξ_s, η_s stand for distances between points O_n and S in the direction of axes $O_n\xi$ and $O_n\eta$. At the shear center, warping W_s is zero, therefore strain $\varepsilon_x$is evaluated again by replacing Eq.(1.21) into Eq.(1.25):

$$\varepsilon_x = -\left[\left(\rho_y' - \rho_y\right)\eta_S + \left(\rho_z' - \rho_z\right)\xi_S\right] \tag{1.26}$$

By substituting Eq.(1.16) and Eq.(1.18) into above, we can obtain relationship among displacements u, v, w and β as following:

$$\frac{1}{R_S}\frac{du}{ds} = \frac{1}{1+\left(\frac{\eta_S}{R_S}\sin\alpha + \frac{\xi_S}{R_S}\cos\alpha\right)}\left[\frac{1}{R_S}\left(\rho_z v - \rho_y w\right) + \beta\left(\frac{\xi_S}{R_S}\sin\alpha - \frac{\eta_S}{R_S}\cos\alpha\right) - \frac{\xi_S}{R_S}\frac{d^2v}{ds^2} + \frac{\eta_S}{R_S}\frac{d^2w}{ds^2}\right] \tag{1.27}$$

Now the relationship between forces and displacements can be achieved by making use of Eq.(1.27)in Eq.(1.16) and substituting into Eq.(1.21):

$$E_s I_\eta' \begin{bmatrix} \frac{d^4v}{ds^4} + \frac{1}{R_s^2}\frac{d^2v}{ds^2} + \left(\rho_y\rho_z\right)^2\left(1 - \frac{I_\eta'}{I_\eta'}\right)v - \\ \rho_y\rho_z\left(1 - \frac{I_\xi'}{I_\eta'}\right)\left(\frac{d^2w}{ds^2} + \rho_y^2 w\right) - \\ \rho_y\left\{\frac{d^2\beta}{ds^2} + \left(\rho_y^2 + \rho_z^2\frac{I_\xi'}{I_\eta'}\right)\beta\right\} \end{bmatrix} = \frac{R_P}{R_S}\left[q_{\bar{y}} - \rho_y\left(\tau_{\bar{x}} - z_P q_{\bar{y}} + y_P q_{\bar{z}}\right)\right] \tag{1.28}$$

$$E_s I_\xi{}' \begin{bmatrix} \dfrac{d^4 w}{ds^4} + \dfrac{1}{R_s^2}\dfrac{d^2 w}{ds^2} + \left(\rho_y \rho_z\right)^2 \left(1 - \dfrac{I_\eta{}'}{I_\xi{}'}\right) w - \\ \rho_y \rho_z \left(1 - \dfrac{I_\eta{}'}{I_\xi{}'}\right)\left(\dfrac{d^2 v}{ds^2} + \rho_z^2 v\right) - \\ \rho_z \left\{\dfrac{d^2 \beta}{ds^2} + \left(\rho_z^2 + \rho_y^2 \dfrac{I_\eta{}'}{I_\xi{}'}\right)\beta\right\} \end{bmatrix} = \frac{R_P}{R_S}\left[q_{\bar{z}} - \rho_z\left(\tau_{\bar{x}} - z_P q_{\bar{y}} + y_P q_{\bar{z}}\right)\right] \tag{1.29}$$

$$E_s C_w \begin{bmatrix} \dfrac{d^4 \beta}{ds^4} + \dfrac{G_s J}{E_s C_w}\dfrac{d^2 \beta}{ds^2} + \left(\rho_z^2 \dfrac{I_\xi{}'}{C_w} + \rho_y^2 \dfrac{I_\eta{}'}{C_w}\right)\beta + \\ \rho_y \left\{\dfrac{d^4 v}{ds^4} - \left(\dfrac{G_s J}{E_s C_w} - \dfrac{I_\eta{}'}{C_w}\right)\dfrac{d^2 v}{ds^2} + \rho_z^2\left(\dfrac{I_\xi{}'}{C_w} - \dfrac{I_\eta{}'}{C_w}\right) v\right\} + \\ \rho_z \left\{\dfrac{d^4 w}{ds^4} - \left(\dfrac{G_s J}{E_s C_w} - \dfrac{I_\xi{}'}{C_w}\right)\dfrac{d^2 w}{ds^2} + \rho_y^2\left(\dfrac{I_\eta{}'}{C_w} - \dfrac{I_\xi{}'}{C_w}\right) w\right\} \end{bmatrix} = \frac{R_P}{R_S}\left(\tau_{\bar{x}} - z_P q_{\bar{y}} + y_P q_{\bar{z}}\right) \tag{1.30}$$

Eccentric distances ξ_S and η_S in ordinary curved bridges are small enough compared with radius of curvature R_S to be neglected, so by omitting those terms in Eq.(1.27), the third term on the right-hand side of the Eq.(1.16) can be described utilizing Eq.(1.3):

$$\begin{aligned} \rho_y \frac{du}{ds} &\cong \rho_y \rho_z v - \rho_y^2 w \\ \rho_z \frac{du}{ds} &\cong \rho_z^2 v - \rho_y \rho_z w \end{aligned} \tag{1.31}$$

Finally, using above equation together with Eq.(1.16) and Eq.(1.21), linearized formulas for stress resultants M_ξ, M_η and T_x:

$$\begin{aligned} T_x &= G_s J\left(\frac{d\beta}{ds} + \rho_y \frac{dv}{ds} + \rho_z \frac{dw}{ds}\right) - E_s C_w\left(\frac{d^3\beta}{ds^3} + \rho_y \frac{d^3 v}{ds^3} + \rho_z \frac{d^3 w}{ds^3}\right) \\ M_\xi &= -E_S I_\xi{}'\left(\frac{d^2 w}{ds^2} + \rho_y^2 w - \rho_y \rho_z v - \rho_z \beta\right) \\ M_\eta &= E_S I_\eta\left(\frac{d^2 v}{ds^2} + \rho_z^2 v - \rho_y \rho_z w - \rho_y \beta\right) \end{aligned} \tag{1.32}$$

Whereas $I_\xi{}'$ and $I_\eta{}'$ are:

$$\begin{aligned} I_\xi{}' &= \frac{R_S}{R_O} I_\xi \\ I_\eta{}' &= \frac{R_S}{R_O} I_\eta \end{aligned} \tag{1.33}$$

So far, the theoretical representation of statics has been described through various mathematical manipulations and rational assumptions. However, finding solution for stress resultants might be still challenging. Therefore, further simplification is needed.

First, let us specify the components of arbitrary load q in the direction of $P\bar{y}$ and $P\bar{z}$ as shown in the Figx:

$$\begin{aligned} q_{\bar{y}} &= q\sin\alpha \\ q_{\bar{z}} &= q\cos\alpha \end{aligned} \tag{1.34}$$

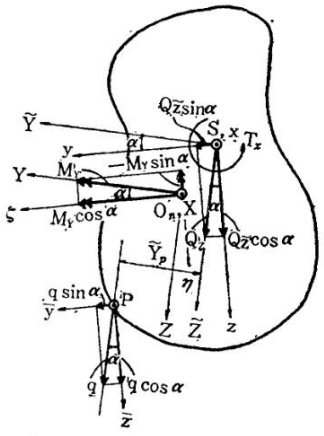

Fig 2.6. Analysis of forces and stress resultants.

The same can be applied for shearing force $Q_{\hat{z}}$ acting along the vertical axis $S_{\hat{z}}$ and subdividing it into two shearing forces Q_y and Q_z:

$$\begin{aligned} Q_y &= Q_{\hat{z}}\sin\alpha \\ Q_z &= Q_{\hat{z}}\cos\alpha \end{aligned} \tag{1.35}$$

Likewise, the bending moment M_Y about horizontal axis $O_\eta Y$ is resolved into two bending moments M_ξ and M_η:

$$\begin{aligned} M_{\xi} &= M_Y\cos\alpha \\ M_{\eta} &= -M_Y\sin\alpha \end{aligned} \tag{1.36}$$

If we substitute last three equation into Eq.(1.4) and Eq.(1.15), $Q_{\hat{z}}$ will be reduced to:

$$\frac{dQ_{\hat{Z}}}{ds} = -\frac{R_P}{R_S}q \tag{1.37}$$

Moreover, by using Eq.(1.1), M_Y can be rewritten as below:

$$\frac{d^2M_Y}{ds^2} + \frac{M_Y}{R_S^2} = -\left(\frac{R_P}{R_S}\right)^2 q \tag{1.38}$$

As it can be clearly seen that moment and shear can be solved separately. By applying Eq.(1.1), Eq.(1.34), and Eq.(1.36) into Eq.(1.15) and also by using above expression for M_Y, we can obtain

differential equations for torsional moment T_x whereas $\widehat{Y_P}$ means the horizontal distance between S and P:

$$\frac{dT_x}{ds} = \frac{M_Y}{R_S} - \frac{R_P}{R_S}\hat{Y}_P q \tag{1.39}$$

Next chapters contain the solution for determining M_Y and T_x by introducing appropriate boundary conditions. Nevertheless, by using above equation, as well as Eq.(1.21) and Eq.(1.24), the warping moment M_w can be derived:

$$\frac{d^2M_w}{ds^2} - \frac{G_s J}{E_s C_w} M_w = \frac{R_O}{R_S}\hat{Y}_P q - \frac{M_Y}{R_S} \tag{1.40}$$

If we assume M_Y is known, warping moment is found again by using boundary conditions. Recalling the Eq.(1.22) and Eq.(1.23), torsional angle can be easily determined:

$$\theta = \iint \frac{M_w}{E_s C_w} ds^2 + C_1 + C_2 \tag{1.41}$$

Once we know M_ξ, $M_\eta$and θ, the simplified form of relation between stress resultants and displacement is achieved by making use of Eq.(1.16) and Eq. (1.21):

$$\begin{aligned} \frac{d^2v}{ds^2} + \frac{v}{R_S^2} &= \frac{M_\eta}{E_s I_\eta} + \rho_y \theta \\ \frac{d^2w}{ds^2} + \frac{w}{R_S^2} &= -\frac{M_\xi}{E_s I_\eta} + \rho_z \theta \end{aligned} \tag{1.42}$$

Up to this point, the methodology of solving the static problem in curved girders has been clearly demonstrated and practical formulas are provided. Following sections govern the dynamic behavior of the curved girder and different approaches to obtain equation of motion girder with curvature.

2.2.5 Solution for Moment

In order to determine the external moment M_Y from Eq.(1.38), let's suppose $R_P \cong R_S = R$ since the vertical load is acting symmetrically (e.g the P point is located in center), so the difference between point P and S is negligible. Next, we denote semi-angle as $\varphi_0 = \varphi/2$, knowing that $s = R \cdot \varphi$, the Eq. (1.38) reduces to:

$$\frac{d^2M_Y}{d\varphi^2} + M_Y = -q \cdot R^2 \tag{1.43}$$

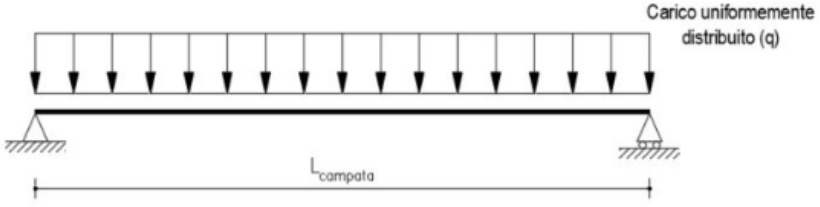

Fig 2.7. Simply supported beam (front view).

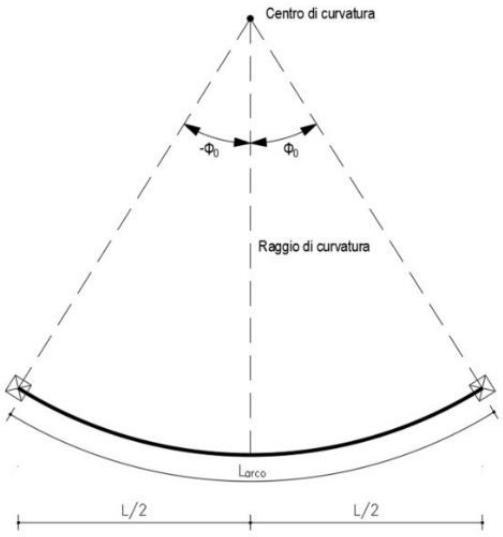

Fig 2.8. Simply supported beam (top view).

The general solution of this linear differential equation is:

$$M_Y = C_1 \cos\varphi + C_2 \sin\varphi - qR^2 \tag{1.44}$$

See appendix 1 for derivation. For simply supported curved bridge deck, using boundary conditions, one is able to determine constants C_1 and C_2:

$$\varphi = 0, M_Y = 0 \rightarrow C_2 R^2 p = 0 \tag{1.45}$$

$$\varphi = \varphi/2, M_Y = 0 \rightarrow C_1 \cos(\varphi/2) - C_2 \sin(\varphi/2) - qR^2 = 0 \tag{1.46}$$

Solving for $C_1$and C_2 and replacing it in the general solution, one obtains:

$$M_Y = qR^2 \left(\frac{\cos\varphi}{\cos(\varphi_0)} - 1 \right) \tag{1.47}$$

Below comparison illustrates the way of expression bending moment of curved girder in terms of equivalent bending moment in a straight girder:

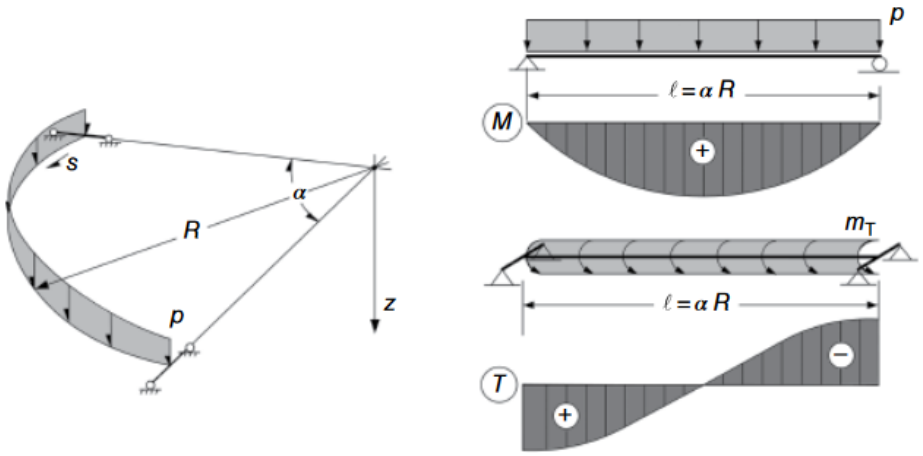

Figure 2.9. Simplified method for moment determination in curved bridge girder.

$$M_Y = qR^2\left(\frac{\cos\varphi}{\cos(\varphi_0)} - 1\right) = M_{eq}\frac{8}{\varphi^2}\left(\frac{\cos\varphi}{\cos\varphi_0} - 1\right) \tag{1.48}$$

The effect of the curvature on the calculation of bending moments might be ignored for the most practical bridge applications, so the transformation of the curved deck to an equivalent straight deck of span length equal to the arc length gives similar results in small errors. For example, single simply supported beam with constant in-plan radius, under uniformly distributed load, the error for maximum bending moment is no more than 1% for aperture angles less than 17 degrees.

2.2.6 Solution for Torsion using Approximate Method

Reis and Pedro has introduced approximation method where they consider an element of a curved beam with infinitesimal length under uniform vertical load and torque, so equilibrium equation of free body diagram is:

$$\sum F_z = -V + V + dV + q\cdot ds = 0$$

$$dV + q\cdot ds = q\cdot r\cdot d\varphi + dV = 0 \rightarrow q = -\frac{dV}{rd\varphi} \tag{1.49}$$

Moment balance equation around perpendicular axis:

$$-M_Y + (M_Y + dM_Y)\cos d\varphi + (T_x + dT_x)\sin d\varphi - (V - dV)ds - q\cdot ds\cdot\frac{ds}{2} + m_t\cdot ds\cdot\sin d\varphi = 0$$

whereas $\cos d\varphi \approx 1$ and $\sin d\varphi \approx d\varphi$, we obtain:

$$-V\cdot ds + dM_Y + T_x d\varphi = -V\cdot r\cdot d\varphi + dM_Y + T_x d\varphi = 0 \rightarrow \frac{dM_Y}{rd\varphi} = V - \frac{T_x}{r} \tag{1.50}$$

Moment balance equation around longitudinal axis:

$$-T_x + (T_x + dT_x)\cos d\varphi - (M_Y + dM_Y)\sin d\varphi + (V - dV)ds\sin d\varphi + qds\frac{ds}{2}\sin d\varphi +$$

$$m_t ds\cos d\varphi = 0$$

$$m_t \cdot ds - M_Y d\varphi + dT_x = m_t \cdot r \cdot d\varphi - M_Y d\varphi + dT_x = 0 \rightarrow \frac{dT_x}{r d\varphi} = \frac{M_Y}{r} - m_t \tag{1.51}$$

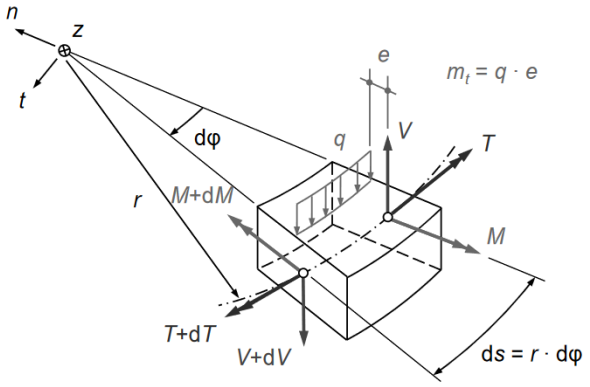

Figure 2.10. Infinitesimal part of curved beam

By adding external torque into Eq.(1.43) and in case $r \neq const$, the differential equation can be solved by considering straight beam with span length of $s = r \cdot \varphi$:

$$\frac{d^2 M_Y}{d\varphi^2} = \frac{m_t}{r} - \frac{M_Y}{r^2} - q \tag{1.52}$$

Often, we have $|q| \gg \left|\frac{M_Y}{r^2}\right|$, therefore the equation can be illustrated as:

$$\frac{d^2 M_Y}{d\varphi^2} \approx \frac{m_t}{r} - q \tag{1.53}$$

The moment M_Y is determined through iteration until convergence is achieved. Similarly, T can be determined as well using Eq.(1.51):

$$\frac{dT}{d\varphi} = M_Y - m_t \cdot r \rightarrow \frac{dT}{ds} = \frac{M_Y}{r} - m_t \tag{1.54}$$

This method is applicable both for single span and continuous bridge decks.

Another approach is 3D finite element method which is more general and comprehensive and allows modelling complex geometries (sharp and/or variable curvature, skew supports, composite cross-sections). It also provides detailed information of displacement (at various construction stages), accurate analysis of stress and forces, economical solution in terms of optimization of cross-section, material properties etc. In following chapters, the case study is described in which the viaduct is analyzed by finite element software.

2.2.7 Solution for Torsion through Statics

In previous chapters, the simplified method was discussed the to determine torsion and moment in curved decks. However, the torsion was described only at instant point along curved beam and global torsion was not explicitly described with certain parameters. Furthermore, due to the practical reasons, the moment over the radius were neglected in the equation. Recent analysis (Mairone et al.) allows to illustrate the torsion of overall curved beam. In this case, the beam is subjected to vertical load q, without external torsion m_t.

By substituting Eq.(1.54) into Eq.(1.44), one gets:

$$\frac{dT_x}{d\varphi} - C_1 \cos\varphi - C_2 \sin\varphi + qR^2 = 0 \tag{1.55}$$

$$T_x = C_1 \sin\varphi - C_2 \cos\varphi - qR^2\varphi + C_3 \tag{1.56}$$

Constants are determined by applying boundary conditions for torsion and moment:

$$M_Y = 0 \text{ at } \varphi = 0 \tag{1.57}$$

$$T_x = 0 \text{ at } \varphi = 0 \tag{1.58}$$

This one is able to solve the system of equation:

$$\begin{cases} C_1 cos\varphi_0 + C_2 sin\varphi_0 - qR^2 = 0 \\ -C_2 + C_3 = 0 \end{cases}$$

$$C_2 = C_3 = 0 \tag{1.59}$$

$$A = \frac{qR^2}{\cos\phi_0} \tag{1.60}$$

Replacing these coefficients into the torsion equation we get:

$$T_x = qR^2 \left[\frac{\sin\varphi}{\cos\varphi_0} - \varphi \right] \tag{1.61}$$

As it can be seen from the above expression, the torsion of a curved girder can be represented separately from moment.

2.2.8 Dynamics of curved beam.

2.2.8.1 Governing equation of motion of curved beam

The Timoshenko beam theory is commonly employed to analyze the dynamic behavior of horizontally curved beams. This method extends beyond basic assumptions by accounting for shear deformation and rotational inertia effects, making it particularly suitable for beams with relatively thin walls and lower shear and torsional rigidity.

In essence, Timoshenko beam is the enhanced version of Euler Bernoulli beam incorporating shear deformation and rotational inertia, making it more accurate for beams where these effects are significant, such as short beams or those with thick cross-sections. Suzuki and Takahashi (1981) compared the natural frequencies and mode shapes in out of plane of clamped curved bars using Timoshenko theory with the classical beam theory. Later, Irie et al. (1982) studied the free vibration of curved arcs considering all types of boundary conditions.

However, in our specific case, the beam exhibits high torsional rigidity and can be classified as a slender beam. Given these characteristics, we can effectively use the simpler Euler-Bernoulli beam theory for our analysis. Earlier, Pang (1966) investigated the behavior of curved beam under the both free and forced vibration solving the equation of motion based on classical beam theory. Previously, the static balance equation was already derived using Euler Bernoulli beam method, by adding kinematic terms into Eq.(1.50) and Eq.(1.51), one is able to construct the equation of motion of curved beam:

$$\frac{\partial T_x}{r\partial\varphi} - \frac{M_Y}{r} = \rho A a^2 \frac{\partial^2 \beta}{\partial t^2} \tag{1.62}$$

$$q - \frac{\partial V}{r\partial\varphi} = \rho A \frac{\partial^2 w}{\partial t^2} \tag{1.63}$$

Note that the sign convection for shear is changed in this case and a is the radius of gyration. Differentiating Eq.(1.62) once with respect to φ and substituting it into Eq.(1.63) gives:

$$\frac{\partial^2 M}{R^2\partial\theta^2} + \frac{\partial T}{R^2\partial\theta} + \rho A \frac{\partial^2 w}{\partial t^2} = q(s,t) \tag{1.64}$$

Replacing the Eq.(1.42) and Eq.(1.32) for torsion into Eq.(1.62) and Eq.(1.64) and collecting like terms leads to the following differential equations:

$$\left(EI + \frac{EC_w}{R^2}\right)\frac{\partial^4 w(s,t)}{\partial s^4} - \frac{GJ}{R^2}\frac{\partial^2 w(s,t)}{\partial s^2} - \left(\frac{EI+GJ}{R}\right)\frac{\partial^2 \beta(s,t)}{\partial s^2} - \frac{EC_w}{R}\frac{\partial^4 \beta(s,t)}{\partial s^4} + \rho A \frac{\partial^2 w(s,t)}{\partial t^2} = q(s,t) \tag{1.65}$$

$$-\left(\frac{EI+GJ}{R}\right)\frac{\partial^2 w(s,t)}{\partial s^2} + \frac{EC_w}{R}\frac{\partial^4 w(s,t)}{\partial s^4} - GJ\frac{\partial^2 \beta(s,t)}{\partial s^2} - \frac{EI}{R^2}\beta + \frac{EC_w}{R}\frac{\partial^4 \beta(s,t)}{\partial s^4} + \rho A a^2 \frac{\partial^2 \beta(s,t)}{\partial t^2} = 0 \tag{1.66}$$

Obtained equation of motions will be further used and solved through eigenvalue problems applying boundary conditions in next chapters.

2.2.8.2 Frequency determination for curved beam

Analysis of out-of-plane vibration frequencies of curved beams has been a subject of continuous interest due to its critical importance in structural engineering, aerospace, and mechanical systems. There are extensive research and many literatures about the natural frequencies of straight and curved beam and only few of them will be discussed in this thesis. This section reviews the key methodologies and findings in the field as outlined in the seminal works and recent research contributions.

The foundational work by Culver (1967) provided earlier exploration into determining the natural frequencies of curved beams by applying Rayleigh-Ritz method which become important sources of comparison for subsequent studies. In structural mechanics, this method is used to approximate the natural frequencies and mode shapes of the structures. It assumes a trial solution for displacement field of the structure expressed as a sum of assumed shape functions that satisfy certain boundary conditions. Next, those functions are substituted into the energy expression (kinetic and potential) of the system resulting eigenvalue problem and eigenvalues corresponds to the squared natural frequencies of a structure such as beam or plates.

Significant advancement in the field of structural dynamics was done by the works of Toshihiro Irie et al. (1982) where he analyzed out of plan vibration of arcs focusing on transfer matrix method. The author was able to derive frequency equation by setting up the problem as a series of matrix differential equation. He proposed formulas of frequency parameters that takes into account various boundary conditions. The numerical analysis provided detailed understanding of dynamic properties of curved bars and allows systematically compare how different assumptions impacts to vibrational characteristics of curved beams.

Another method so called Wittrick Williams Algorithm is the relevant in the context of frequency. The algorithm operates on the principle of systematically bracketing and zeroing in eigenvalues of a system (Howson et al. 1993). It starts by establishing an initial range where eigenvalues are expected to lie and then iteratively narrows down these ranges. This process known as interval bisection combined with Strum sequence property of eigenvalue problems to determine eigenvalues which represents the frequency. The advantage of this method is robustness in converging towards the correct eigenvalues.

The Difference Quadrate Method was effectively used by Kang et al. (1995) to analyze the vibration in horizontally curved beams with warping. DQM is well known for its precision and efficiency in handling complex geometrical and boundary conditions. It simplifies the differential equation of motion by discretizing them into a system of algebraic equations which can be solved numerically providing high degree of accuracy with less computational effort compared to traditional finite element methods.

One of the latest works in determining the frequency of beams is the application of dynamic Green's method explored by Abu-Hilal (2003) . This is a mathematical concept used to solve inhomogeneous differential equations. The author determined dynamic response of prismatic damped Euler-Bernoulli beam subjected to various loading conditions. The paper details the derivation of Green functions which represents the response of a system to a point source of impulse providing the exact solution in closed form.

Above examples are the few works among the other numerous investigations of dynamic behavior of beams. In this thesis, simplified approaches were adopted to calculate the frequency of curved beam using classical beam theory, however it is highly advantageous for the future research to validate the numerical results through comparative analyses with the aforementioned techniques.

Assuming the rotational inertial term being zero in the Eq.(1.66), the vibration frequencies of curved beam can be expressed in terms of the free vibration frequencies of straight beam which has the same length and flexural rigidity as curved beam (Pang 1937):

$$\omega_{bm} = \lambda_i^2 \sqrt{\frac{EI}{\rho A}} K_i \tag{1.67}$$

Where:

$$K_i = 1 + \frac{A}{\lambda_i^2} + \frac{1+A}{1+A\lambda_i^2} \tag{1.68}$$

$$A = \frac{GJ + EC_w \left(\lambda'_i\right)^2}{EI} \tag{1.69}$$

$$\lambda'_i = \frac{i\pi}{R\varphi} \tag{1.70}$$

$$\lambda_i = \frac{i\pi}{\varphi} \tag{1.71}$$

In conclusion, the derived formulas above for the natural frequencies of horizontally curved beam provide a fundamental basis to understand the dynamic behavior of a beam and are crucial for predicting vibrations in such elements.

Chapter 3

3 Case Study

3.1.1 Overview

In this thesis, the model proposed by X. Yin (2015) will be examined as a case study. Two span continuous beam bridges with rubber bearings are investigated. According to the principles of equal-stiffness, different cross section can be displaced equivalently. The girder, pier and rubber bearing are considered to be simply supported curved beam, clamped rod and linear elastic spring, respectively. As shown in Fig.3.1, the simply supported curved beam has length $2s_0$, cross-section area A, Young's modulus E, area moment of inertia I and mass density ρ. The clamped rod has length L, cross-section area A_r, Young's modulus E_r and mass density ρ_r. The gravity of the bridge acting upon the beam is modeled as a linear loading q. The vertical ground motion excited at point A, D and B in Fig.3.1 are represented as $B1(t)$, $B2(t)$ and $B3(t)$, respectively. It should be noted that the primary objective of this thesis is to develop a theoretical approach for investigating the vertical pounding responses of bridge structures under vertical ground motion, although the horizontal motions will cause bridge structures to vibrate and the responses induced by horizontal and vertical ground motions are coupled; for clear observations of the effects of vertical ground excitations, in this study only the vertical ground excitations are considered. Further study to investigate the coupled effects of horizontal and vertical ground motions on vertical pounding responses between bridge girders and supports is deemed necessary. Moreover, although damages to bridge pier and bearings owing to vertical poundings have been observed in previous earthquakes, to avoid further complicate the problem and allow the study concentrate on investigating the influences of vertical pounding on bridge responses, in the present study material nonlinearity is not considered.

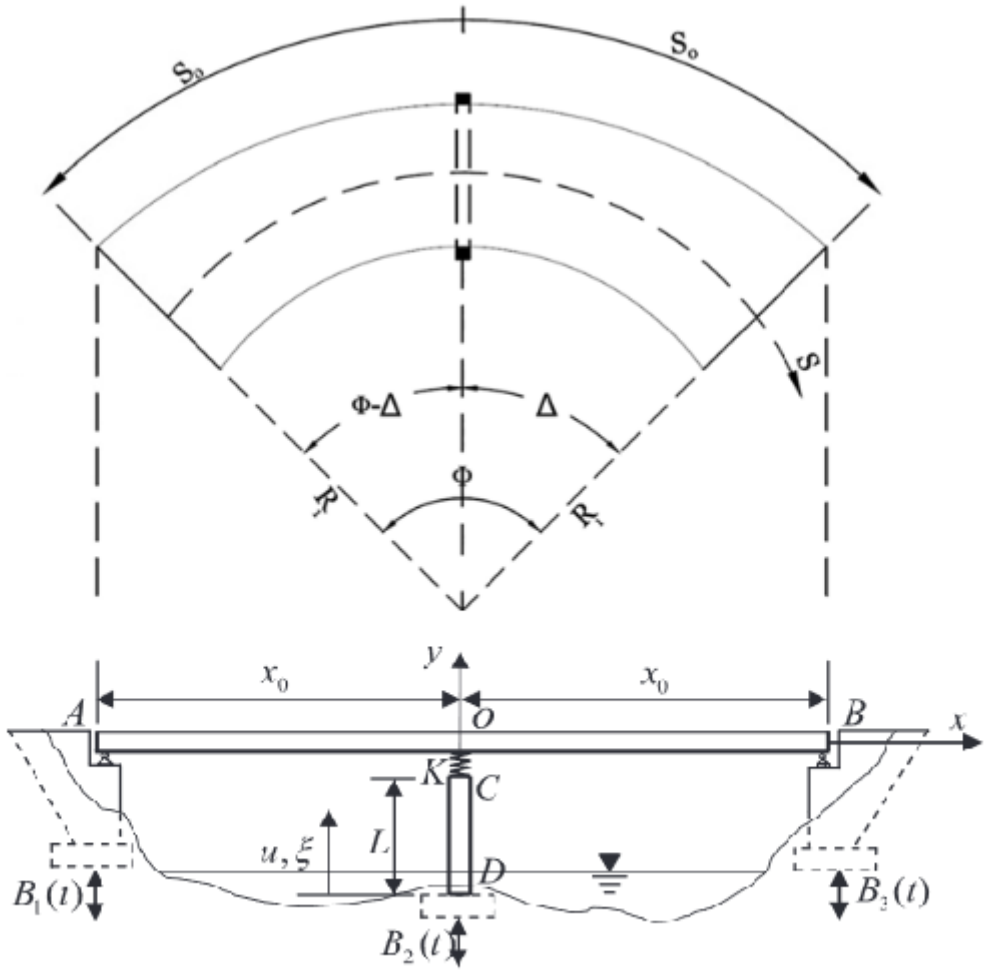

Fig 3.1. Two-span continuous bridge model

During vertical ground movement, the bridge's response has three stages:

1. Pre-separation: The initial contact between the beam and the bearing is reserved, therefore the beam vibrates at the same frequency w_n with the rod.
2. Separation: The beam is no longer in contact with the bearing which cause the different vibration of w_{bn} and w_{rn} for the beam and the rod respectively.
3. Pounding: The beam comes into contact with the bearing again as in first phase making the beam and the rod to vibrate at the same frequency w_n.

During the pounding process, the pounding force F is generated between the girder and the bearing. Generally, the stereo-mechanical approach and the contact element approach are used to analyze the pounding phenomena in bridge structures under earthquake. The pounding forces obtained from these two models depend on the coefficient of restitution and the damping coefficient, while the selection of these coefficients is difficult because it depends on many factors. In this study, a new theoretical approach of the vertical pounding forces is presented based on the transient internal force on the contact surface of the girder and bearing. In this new approach, there are two main steps to calculate the pounding force. First, the transient responses in the in-contact phase, then, the internal forces, i.e. the internal pressure at the pier end or the spring force, are obtained and form the solution of the transient responses. Therefore, based on the internal force, the pounding force can be found as follows:

$$F(t)=\begin{cases}\iint_{\Gamma_c}\sigma_r dA & t_{2k}\le t\le t_{2k+1}\\ 0 & t_{2k+1}\le t\le t_{2k+2}\end{cases}$$

or

$$F(t)=\begin{cases}K\left(u(L,t)-w_1(0,t)\right) & t_{2k}\le t\le t_{2k+1}\\ 0 & t_{2k+1}\le t\le t_{2k+2}\end{cases} \tag{2.1}$$

The solution for transient wave propagation for in-contact phase contains two parts:

$$w_1(s,t)=w_{1s}(s,t)+w_{1d}(s,t) \tag{2.2}$$

$$w_2(s,t)=w_{2s}(s,t)+w_{2d}(s,t) \tag{2.3}$$

$$\beta(s,t)=\beta_s(s,t)+\beta_d(s,t) \tag{2.4}$$

$$u(\xi,t)=u_s(\xi,t)+u_d(\xi,t) \tag{2.5}$$

Basically, the pounding force is evaluated in terms of static and dynamic displacements of both beam and pier's top. Following chapters show the methods to obtain these displacements with already derived formulas. In addition, the differences between straight beam compared with curved one are pointed out.

3.1.2 Static Solution

3.1.2.1 Vertical quasi-static displacement for in-contact phase

For a straight beam, vertical deflection and applied load along the length x can be described through well-known Euler-Bernoulli equation (Gere 2011):

$$EI\frac{d^4w(x)}{dx^4}=q(x) \tag{2.6}$$

Rewriting the Eq.(1.42):

$$\frac{d^2w(s)}{ds^2}+\frac{w(s)}{R_S^2}=-\frac{M_\xi}{E_sI_\eta}+\frac{\cos\alpha}{R_S}\theta \tag{2.7}$$

As most of the bridges, the bridge girder under study is not inclined, so $\alpha=0$. Since $R=R_S\cong R_P$ is significantly higher than vertical deflection w and rotation θ, the second terms of both right and left hand side of the equation can be neglected. Moreover, let's denote rigidity parameters $E_\eta I_\eta$ as simpler form *EI* because we consider only vertical load and displacements. By substituting Eq.(1.36) into above, we get:

$$\frac{d^2w(s)}{ds^2}=-\frac{M_Y}{EI} \tag{2.8}$$

If we replace previously calculated moment M_Y in Eq.(1.47) into above, the deflection can be evaluated as a function of radius and angle of the curvature:

$$\frac{d^2w(s)}{ds^2}=-\frac{qR^2}{EI}\left(\frac{\cos\varphi}{\cos\varphi_0}-1\right) \tag{2.9}$$

The solution can be found by twice integrating the equation and introducing boundary conditions to determine constant coefficients:

$$\frac{dw(s)}{ds} = -\frac{qR^2}{EI}\left(\frac{\cos\varphi}{\cos\varphi_0} - 1\right)s + C_0$$

$$w(s) = -\frac{qR^2}{EI}\left(\frac{\cos\varphi}{\cos\varphi_0} - 1\right)\frac{s^2}{2} + C_0 s + C_1 \tag{2.10}$$

Deflection at both ends of curved beam is equal to zero:

$$w_1(-s_0) = 0 \tag{2.11}$$

$$w_2(s_0) = 0 \tag{2.12}$$

$C_0 = 0$ and

$$C_1 = \frac{qR^2}{EI}\left(\frac{\cos\varphi}{\cos\varphi_0} - 1\right)\frac{s_0^2}{2} \tag{2.13}$$

Obtaining these integrant constants one can reconstruct the vertical deflection expression for the beam *OA* due to the linear loading q.

$$w_1(s) = \frac{q}{2EI}\left(\frac{\cos\varphi}{\cos\varphi_0} - 1\right)\left[s_0^2 - s^2\right] \tag{2.14}$$

However, there is also the contribution of static contact force F on vertical deflection and from balance equation at the mid-span we know that:

$$-V + 2F = 0 \tag{2.15}$$

Substituting above expression into Eq. (1.5) and then into (1.42) we can relate shear and displacement by following:

$$\frac{d^3 w_1(s)}{ds^3} = -\frac{V_1}{EI} = -\frac{2F}{EI} \tag{2.16}$$

$$\frac{d^2 w_1(s)}{ds^2} = -\frac{F}{EI}s + C_0$$

$$\frac{dw_1(s)}{ds} = -\frac{F}{EI}\frac{s^2}{2} + C_0 s + C_1$$

$$w_1(s) = -\frac{F}{EI}\frac{s^3}{6} + C_0\frac{s^2}{2} + C_1 s + C_2 \tag{2.17}$$

Boundy conditions are following:

$$\frac{dw_1(-s_0)}{ds} = \frac{dw_2(s_0)}{ds} \tag{2.18}$$

$$\frac{dw_1(-s_0)}{ds} = 0 \tag{2.19}$$

$$w_1(-s_0) = 0 \tag{2.20}$$

Setting the right boundary conditions, one is able to determine integration constants again:

$$C_0 = 0$$

$$C_1 = \frac{F}{EI}\frac{s_0^2}{2}$$

$$C_2 = \frac{F}{EI}\frac{s_0^3}{3}$$

So, the vertical deflection of the curved beam OA due to the F will be:

$$w_1(s) = \frac{F}{6EI}\left(2s_0^3 - s^3 + 3s_0^2 s\right) \tag{2.21}$$

The total static vertical deflection of the curved beam OA becomes:

$$w_1(s) = \frac{\left(3qR^2\left(\frac{\cos\varphi}{\cos\varphi_0} - 1\right)\left[s_0^2 - s^2\right] + F\left[2s_0^3 - s^2 + 3s_0^2 s\right]\right)}{6EI} \tag{2.22}$$

Similarly, the displacement of OB due to the loading q is the same as in case OB while displacement due to the contact force F differ according to boundary conditions together with (2.18):

$$\frac{dw_2(s_0)}{ds} = 0 \tag{2.23}$$

$$w_1(s_0) = 0 \tag{2.24}$$

Coefficients C_0, C_1 and C_2 are:

$$C_0 = 0$$

$$C_1 = \frac{F}{EI}\frac{s_0^2}{2}$$

$$C_2 = -\frac{F}{EI}\frac{s_0^3}{3}$$

Therefore, the vertical deflection of the curved beam OB due to the F:

$$w_2(s) = \frac{F}{6EI}\left(-2s_0^3 - s^3 + 3s_0^2 s\right) \tag{2.25}$$

The total static vertical deflection of the curved beam OB:

$$w_2(s)=\frac{\left(3qR^2\left(\frac{\cos\varphi}{\cos\varphi_0}-1\right)\left[s_0^2-s^2\right]+F\left[2s_0^3+s^2-3s_0^2s\right]\right)}{6EI} \tag{2.26}$$

On the other hand, longitudinal displacement of the rod is:

$$u(\xi)=\frac{F}{E_rA_r}\xi \tag{2.27}$$

Chai Hong Yoo (1986) suggests that if the dimensionless coefficient L^2GJ/EC_w is larger than 100, the contribution of warping effect to the lateral buckling can be neglected both for straight and curved beams as in Fig.3.2.

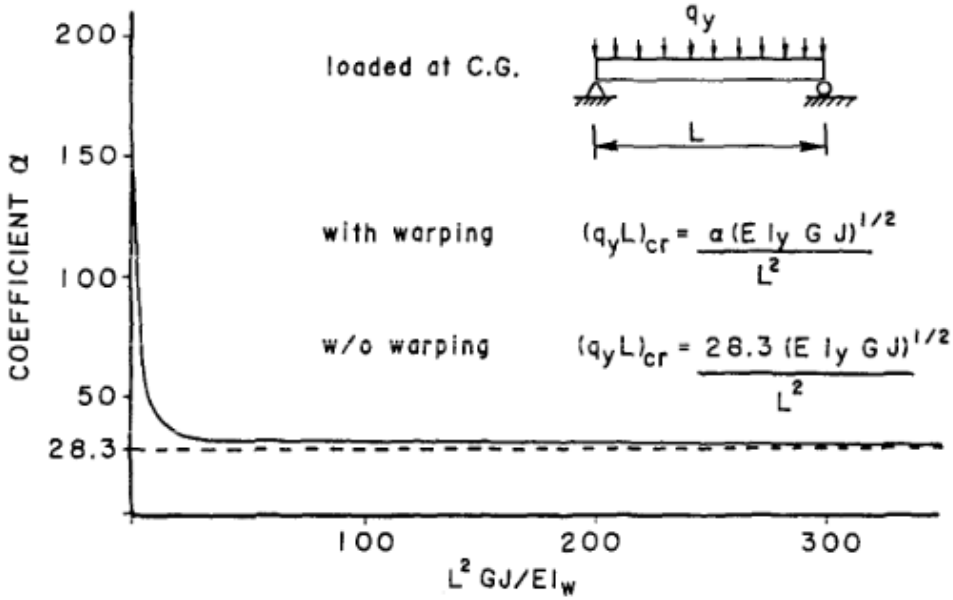

Fig 3.2. Warping contribution to lateral buckling

In next chapters, given all parameters of the bridge (material properties, dimensions and etc) this coefficient can be easily calculated and it is equal to 2586112, which is much higher than 100, meaning that one can surely ignore the warping wherever in solving static or dynamic problems. Hence, the Eq.(1.21) simplifies to:

$$T_x=G_sJ\frac{d\theta}{ds} \tag{2.28}$$

Above variables are the initial displacements in pre-separation phase (at $t=0$). Finding torsional angle θ by using Eq.(1.61) and substituting it into (1.42), we can now input vertical ground motion in terms of displacements, for simplicity, let's add the sum and difference of $B1(t), B2(t)$ and $B3(t)$:

$$w_1(s,t)=\frac{qR^2\left(\frac{\cos\varphi}{\cos\varphi_0}-1\right)\left[s_0^2-s^2\right]}{2EI}-\frac{qR\left(\frac{\sin\varphi}{\cos\varphi_0}-\varphi\right)\left[2s_0^3-s_0s^2-s^3\right]}{2GJ}+ \\ \frac{F\left[2s_0^3-s^2+3s_0^2s\right]}{6EI}-\frac{B_1(t)-B_3(t)}{2s_0}s+\frac{B_1(t)+B_3(t)}{2} \tag{2.29}$$

$$w_2(s,t)=\frac{qR^2\left(\frac{\cos\varphi}{\cos\varphi_0}-1\right)\left[s_0^2-s^2\right]}{2EI}-\frac{qR\left(\frac{\sin\varphi}{\cos\varphi_0}-\varphi\right)\left[2s_0^3-s_0s^2-s^3\right]}{2GJ}+ \\ \frac{F\left[2s_0^3+s^2-3s_0^2s\right]}{6EI}-\frac{B_1(t)-B_3(t)}{2s_0}s+\frac{B_1(t)+B_3(t)}{2} \tag{2.30}$$

$$u(\xi,t)=\frac{F(t)}{E_rA_r}\xi+B_2(t) \tag{2.31}$$

In order to determine force $F(t)$, we apply the continuity condition for shearing force and displacement between beam and spring for in-contact case:

$$u(L,t)-w_1(0,t)=\delta=\frac{F}{K}=-\frac{E_rA_r}{K}\frac{\partial u(L,t)}{\partial\xi} \tag{2.32}$$

By substituting Eq.x into continuity condition, dynamic contact forced between bearing and girder can be easily found:

$$F(t)=\frac{qR^2s_0^2\left(\cos\varphi/\cos\varphi_0-1\right)/2EI+\left(B_1(t)+B_3(t)\right)/2-B_2(t)}{L/E_rA_r-s_0^3/3EI-1/K} \tag{2.33}$$

Note that initial velocity of the beam and the rod in pre-separation are:

$$\frac{\partial w_1(s,0)}{\partial t}=0 \tag{2.34}$$

$$\frac{\partial w_2(s,0)}{\partial t}=0 \tag{2.35}$$

$$\frac{\partial u(\xi,0)}{\partial t}=0 \tag{2.36}$$

3.1.2.2 Vertical quasi-static displacement for out-of-contact phase

Up to now, the static solution was provided only for in-contact phase. Due to the support conditions changes when the girder is separated from the pier, there is no contact force *F* acting beneath. Moreover, the girder may rotate about its longitudinal axis because of coupling with vertical displacement. Determining the static rotation can be performed either by solving Eq.(1.41) or by Eq.(1.21).

the vertical quasi-static displacement $w_{bs}(s,t)$ for out-of-contact phase by making use of the same boundary condition as in contact phase except those in the mid-span.

$$w_{bs}(s,t)=\frac{qR^2\left(\frac{\cos\varphi}{\cos\varphi_0}-1\right)\left[s_0^2-s^2\right]}{2EI}-\frac{qR\left(\frac{\sin\varphi}{\cos\varphi_0}-\varphi\right)\left[2s_0^3-s_0s^2-s^3\right]}{2GJ}$$
$$-\frac{B_1(t)-B_3(t)}{2s_0}s+\frac{B_1(t)+B_3(t)}{2} \tag{2.37}$$

Now quasi-static rotation of the girder can be easily determined by substituting above into Eq.(1.17):

$$\beta_{bs}(s,t)=\frac{-qR\left(\frac{\cos\varphi}{\cos\varphi_0}-1\right)\left[s_0^2-s^2\right]}{2EI}+\frac{q\left(\frac{\sin\varphi}{\cos\varphi_0}-\varphi\right)\left[2s_0^3-s_0s^2-s^3+2R^2\left(s+s_0\right)\right]}{2GJ}$$
$$+\frac{B_1(t)-B_3(t)}{2s_0}s-\frac{B_1(t)+B_3(t)}{2} \tag{2.38}$$

3.1.3 Dynamic Solution

3.1.3.1 Vertical dynamic displacement for in-contact phase

Second part of the problem can be understood as a summation of infinite series of the product of time function $q_n(t)$ and the wave modes specific to both the girder (flexural modes for the beam φ_{bn1} and φ_{bn2}) and the pier (longitudinal modes for the rod φ_{rn}). Each mode describes a distinct pattern of how the beam bends or how the rod stretches over time.

$$w_{1d}(s,t)=\sum_{n=1}^{\infty}\phi_{bn1}(s)q_n(t)$$
$$w_{2d}(s,t)=\sum_{n=1}^{\infty}\phi_{bn2}(s)q_n(t) \tag{2.39}$$
$$u_d(\xi,t)=\sum_{n=1}^{\infty}\phi_{rn}(\xi)q_n(t)$$

Boundary conditions of the two-span bridge in the mid-span prevents rotation of the cross-section of the girder $\beta=0$, and assuming the radius of curvature is significantly higher than vertical displacement, the equation of motion of curved beam reduces to the equation of motion of straight beam. The Eq.(1.65) can be rewritten as:

$$EI\frac{\partial^4 w(s,t)}{\partial s^4}+\rho A\frac{\partial^2 w(s,t)}{\partial t^2}=q \tag{2.40}$$

The equation of motion of the pier can be considered as a St. Venant Rod:

$$E_rA_r\frac{\partial^2 u(\xi,t)}{\partial \xi^2}+\rho_rA_r\frac{\partial^2 u(\xi,t)}{\partial t^2}=q \tag{2.41}$$

Substituting Eq.(2.39) into above two equation of motions, the eigenequations of beams and rod are obtained:

$$
\begin{aligned}
a^2 \frac{\partial^4 \phi_{bn1}}{\partial s^4} - \omega_n^2 \phi_{bn1} = 0 \\
a^2 \frac{\partial^4 \phi_{bn2}}{\partial s^4} - \omega_n^2 \phi_{bn2} = 0 \\
c_r^2 \frac{\partial^2 \phi_{rn}}{\partial \xi^2} - \omega_n^2 \phi_{rn} = 0
\end{aligned} \tag{2.42}
$$

where $a = \sqrt{EI/\rho A}$ and $c = \sqrt{E_r/\rho_r}$ is the coefficients associated with the flexural wave speed of the beam and phase speed of the rod. The solution for the flexural wave modes ϕ_{bn} and longitudinal wave mode ϕ_{rn}can be expressed as:

$$
\begin{aligned}
\phi_{bn1} = A_{n1} \sin k_{bn} s + B_{n1} \cos k_{bn} s + C_{n1} \sinh k_{bn} s + D_{n1} \cosh k_{bn} s \\
\phi_{bn2} = A_{n2} \sin k_{bn} s + B_{n2} \cos k_{bn} s + C_{n2} \sinh k_{bn} s + D_{n2} \cosh k_{bn} s \\
\phi_{rn} = E_n \sin k_{rn} \xi + F_n \cos k_{rn} \xi
\end{aligned} \tag{2.43}
$$

where

$$
k_n = [k_{bn}, k_{rn}]^T = \left[\sqrt{\omega_n/a}\,, \omega_n/c\right]^T
$$

$$
A_n^* = [A_{n1}, A_{n2}, B_{n1}, B_{n2}, C_{n1}, C_{n2}, D_{n1}, D_{n2}, E_n, F_n]^T
$$

are the parameter related to frequency and beam-rod wave mode coefficients. Boundary conditions for eigen modes:

$$
\begin{aligned}
\phi_{bn1}(-s_0) = 0, \phi_{bn1}^{''}(-s_0) = 0, \\
\phi_{bn2}(s_0) = 0, \phi_{bn2}^{''}(s_0) = 0, \phi_r(0) = 0 \\
\phi_{bn1}(0) = \phi_{bn2}(0), \phi_{bn1}^{'}(0) = \phi_{bn2}^{'}(0), \phi_{bn1}^{''}(0) = \phi_{bn2}^{''}(0) \\
\phi_{bn1}(0) = \phi_r(L) + \frac{E_r A_r \phi_r^{'}(L)}{K}, EI\left[\phi_{bn1}^{'''}(0) - \phi_{bn2}^{'''}(0)\right] = E_r A_r \phi_r^{'}(L)
\end{aligned} \tag{2.44}
$$

Substituting wave mode functions into above boundary and continuity conditions yields a system of linear algebraic equations in matrix form. Non-trivial solutions are indicated by the determinant of the coefficient matrix being equal to zero which results the beam-rod frequency equation:

$$
E_r A_r k_{nr} \cos k_{nr} L \left(\tan k_{bn} s_0 - \tanh k_{bn} s_0\right) + 4EIk_{bn}^3 \left(\sin k_{nr} L + \frac{E_r A_r k_{rn} \cos k_{rn} L}{K}\right) = 0 \tag{2.45}
$$

System of linear algebraic equations (see Appendix 3) together with mode orthogonality (see Appendix 2) give the coefficients of wave modes meaning that eigenfunctions itself can be determined:

$$
\begin{aligned}
\phi_{bn1} = M_n E_n \left[-\frac{\sin k_b (s + s_0)}{\cos k_b s_0} + \frac{\sinh k_b (s + s_0)}{\cosh k_b s_0}\right] \\
\phi_{bn2} = M_n E_n \left[\frac{\sin k_b (s - s_0)}{\cos k_b s_0} - \frac{\sinh k_b (s - s_0)}{\cosh k_b s_0}\right] \\
\phi_{rn} = E_n \sin k_{rn} \xi
\end{aligned} \tag{2.46}
$$

In order to solve temporal part of the eigenvalue problem, we substitute Eq.(2.39) into Eq.(2.40) and Eq.(2.41) and using orthogonality condition derive time differential equation:

$$\ddot{q}_n(t^*) + \omega_n^2 q_n(t^*) = \ddot{Q}_n(t) \tag{2.47}$$

The solution can be obtained by using Laplace transform:

$$q_n(t^*) = q_n(0)\cos\omega_n t^* + \frac{1}{\omega_n}\dot{q}_n(0)\sin\omega_n t^* + \frac{1}{\omega_n}\int_0^{t^*}\ddot{Q}(t_{2k}+\tau)\sin\omega_n(t^*-\tau)d\tau \tag{2.48}$$

Since the external force is applied through static displacement in terms of B_1, B_2 and B_3 (see Eq.(2.29)), it is necessary to project static displacement onto eigenfunctions to decompose beam's response into a series of eigenmodes of the structure. The projection involves integrating the product of the static displacement and eigenfunctions. Multiplying the eigenmode by static displacement serves to weight the static displacement according to the shape of each eigenmode:

$$\begin{aligned}
q_n(0) &= \int_{-s_{.0}}^{s_0}\rho A\phi_{bn}(s)w_0(s,t_{2k}^-)ds + \int_0^L \rho_r A_r\phi_{rn}(\xi)u_0(\xi,t_{2k}^-)d\xi + Q_n(0)\\
\dot{q}_n(0) &= \int_{-s_{.0}}^{s_0}\rho A\phi_{bn}(s)\dot{w}_0(s,t_{2k}^-)ds + \int_0^L \rho_r A_r\phi_{rn}(\xi)\dot{u}_0(\xi,t_{2k}^-)d\xi + \dot{Q}_n(0)\\
Q_n(t^*) &= -\int_{-s_{.0}}^{0}\rho A\phi_{bn1}(s)w_{s1}(s,t^*)ds - \int_0^{s_0}\rho A\phi_{bn2}(s)w_{s2}(s,t^*)ds - \int_0^L \rho_r A_r\phi_{rn}(\xi)u_s(\xi,t^*)d\xi
\end{aligned} \tag{2.49}$$

where t_{2k} is the initial time of the *k*-th in-contact phase, $t^* = t - t_{2k}$ is the time variable of the *k*-th in-contact phase, $y_0(s,t_{2k}^-), \dot{y}_0(s,t_{2k}^-), u_0(\xi,t_{2k}^-)\ and\ \dot{u}_0(\xi,t_{2k}^-)$ are the initial displacement and velocity which are remaining distribution at the moment of the end of previous phase:

$$\begin{aligned}
w_0(s,t_{2k}^-) &= w_{bs}(s,t_{2k}^-) + \sum_{n=1}^{\infty}\phi_{bm}(s)q(t_{2k}^-)\\
u_0(\xi,t_{2k}^-) &= u_s(\xi,t_{2k}^-) + \sum_{n=1}^{\infty}\phi_{rm}(\xi)q(t_{2k}^-)\\
\dot{w}_0(s,t_{2k}^-) &= \dot{w}_{bs}(s,t_{2k}^-) + \sum_{n=1}^{\infty}\phi_{bm}(s)\dot{q}(t_{2k}^-)\\
\dot{u}_0(\xi,t_{2k}^-) &= \dot{u}_s(\xi,t_{2k}^-) + \sum_{n=1}^{\infty}\phi_{rm}(\xi)\dot{q}(t_{2k}^-)
\end{aligned} \tag{2.50}$$

3.1.3.2 Vertical dynamic displacement for out-of-contact phase

The dynamic behavior of the bridge in out of contact phase is straightforward simply because two system don't vibrate with the same frequency as previously. Although separation time in most case is quite short, nevertheless, in combination with horizontal ground motion just after vertical component, the bridge girder may collapse due to the absence of any friction between pier and girder. Therefore, exact and reliable analytical solutions is required to better understand such phenomena. In this section

the same method is adopted as in-contact phase to solve wave modes, frequencies, coefficients of wave modes and time functions.

Equation of motion for separation phase has been already derived in Eq.(1.65) and Eq.(1.66). It becomes much simpler if the term rotational inertia term $ma^2 \frac{\partial^2 \beta}{\partial t^2}$ since no external rotational load is acting on the beam. The eigenfunctions for separation phase for the beam:

$$\phi_{bm}(s) = A_{bm} \sin k_{bm}(s + s_0) \tag{2.51}$$

where the coefficient A_{bm} is obtained by normalization of the eigenmode:

$$A_{bm} = \frac{1}{\sqrt{\rho A s_0}} \tag{2.52}$$

and k_{bm} is the parameter related to frequency already described in Eq.(1.67):

$$k_{bm} = \sqrt{\frac{\omega_{bm}}{a}} \tag{2.53}$$

The general solution of time function for the curved beam in out of contact phase is:

$$q_{bm}(t^*) = q_{bm}(0)\cos\omega_{bm}t^* + \frac{1}{\omega_{bm}}\dot{q}_{bm}(0)\sin\omega_{bm}t^* + \frac{1}{\omega_{bm}}\int_0^{t^*} \ddot{Q}_{bm}(t_{2k+1}+\tau)\sin\omega_{bm}(t^*-\tau)d\tau \tag{2.54}$$

$$\begin{aligned} q_{bm}(0) &= \int_{-s_{.0}}^{s_0} \rho A \phi_{bm}(s) y_{b0}(s, t_{2k+1}^-) ds + Q_{bm}(0) \\ \dot{q}_{bm}(0) &= \int_{-s_{.0}}^{s_0} \rho A \phi_{bm}(s) \dot{y}_{b0}(s, t_{2k+1}^-) ds + \dot{Q}_{bm}(0) \\ Q_{bm}(t^*) &= -\int_{-s_{.0}}^{s_0} \rho A \phi_{bm}(s) y_{bm}(s, t^*) ds \end{aligned} \tag{2.55}$$

where t_{2k+1} is the initial time of the k-th out-of-contact phase, $t^* = t - t_{2k+1}$ is the time variable of the k-th out-of-contact phase, $y_{b0}(s, t_{2k+1}^-)$ *and* $\dot{y_{b0}}(s, t_{2k+1}^-)$ are the initial displacement and velocity which are remaining distribution at the moment of the end of previous phase:

$$\begin{aligned} w_{b0}(s, t_{2k+1}^-) &= w_1(s, t_{2k+1}^-) + \sum_{n=1}^{\infty} \phi_{n1}(s) q_n(t_{2k+1}^-) \\ \dot{w}_{b0}(s, t_{2k+1}^-) &= \dot{w}_1(s, t_{2k+1}^-) + \sum_{n=1}^{\infty} \phi_{n1}(s) \dot{q}_n(t_{2k+1}^-) \end{aligned} \tag{2.56}$$

The eigenfunctions for separation phase for the rod:

$$\phi_{rm}(s) = A_{rm} \sin k_{rm}\xi \tag{2.57}$$

where the coefficient A_{rm} is obtained by normalization of the eigenmode:

$$A_{rm} = \sqrt{\frac{2}{\rho_r A_r L}} \tag{2.58}$$

and k_{rm} is the parameter related to rod frequency in longitudinal direction:

$$k_{rm} = \frac{\omega_{rm}}{c_r} = \frac{(2m-1)\pi}{2L} \tag{2.59}$$

The general solution of time function for the rod in out of contact phase is:

$$q_{rm}(t^*) = q_{rm}(0)\cos\omega_{rm}t^* + \frac{1}{\omega_{rm}}\dot{q}_{rm}(0)\sin\omega_{rm}t^* + \frac{1}{\omega_{rm}}\int_0^{t^*}\ddot{Q}_{rm}(t_{2k+1}+\tau)\sin\omega_{rm}(t^*-\tau)d\tau \tag{2.60}$$

$$\begin{aligned} q_{rm}(0) &= \int_0^L \rho_r A_r \phi_{rm}(\xi) u_{b0}(\xi, t_{2k+1}^-) d\xi + Q_{rm}(0) \\ \dot{q}_{rm}(0) &= \int_0^L \rho_r A_r \phi_{rm}(\xi) \dot{u}_{b0}(\xi, t_{2k+1}^-) d\xi + \dot{Q}_{rm}(0) \\ Q_{rm}(t^*) &= -\int_0^L \rho_r A_r \phi_{rm}(\xi) u_b(\xi, t^*) d\xi \end{aligned} \tag{2.61}$$

Initial displacement and velocity:

$$\begin{aligned} u_{b0}(\xi, t_{2k+1}^-) &= u_{bs}(\xi, t_{2k+1}^-) + \sum_{n=1}^{\infty}\phi_{rn}(\xi) q_n(t_{2k+1}^-) \\ \dot{u}_{b0}(\xi, t_{2k+1}^-) &= \dot{u}_{bs}(\xi, t_{2k+1}^-) + \sum_{n=1}^{\infty}\phi_{rn}(\xi) \dot{q}_n(t_{2k+1}^-) \end{aligned} \tag{2.62}$$

Quasi-static displacement for the rod:

$$u_{bs}(\xi, t) = B_2(t) \tag{2.63}$$

3.2 Numerical Results

3.2.1 Bridge parameters

In this section, we'll examine the numerical results using a standard highway bridge in China as an example. It is advisable to keep the endpoints of the beam fixed (76 m) and examine the forces that lead to an increased imaginary curvature, reducing the radius of curvature up to the midpoint of the beam (38m). All other parameters such as rigidity and density don't vary. Such method allows to detect critical radius or angle of curvature that may cause damage or very high pounding forces.

The bridge contains single pier that is composed of two circular concrete columns with longitudinal bars as in Fig.3.3.

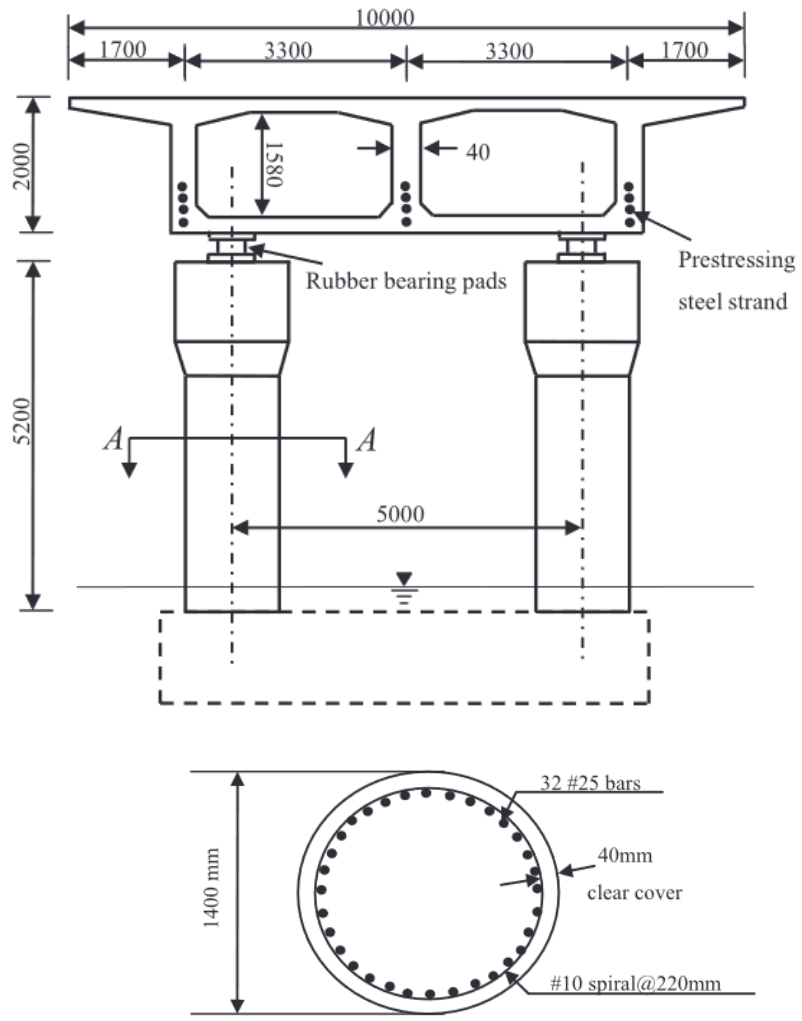

Fig 3.3. Cross-section details of bridge girder and pier

Parameter of bridge girder	
Mass density	$\rho = 2600\ kg/m^3$
Cross-section area	$A_c = 6.04\ m^2$
Young's modulus of concrete	$E_c = 34.5\ GPa$
Inertia moment of girder cross section	$I_c = 3.409\ m^4$
Reinforcement cross-section area	$A_y = 0.04712\ m^2$
Young's modulus of reinforcement	$E_y = 200\ GPa$
Inertia moment of reinforcement cross section	$I_Y = 0.1925\ m^4$
Prestressed steel strand section area	$A_p = 0.02688\ m^2$
Young's modulus of prestressed steel strand cross section	$E_p = 195\ GPa$
Inertia moment of prestressed steel strand cross section	$I_p = 0.07585\ m^4$
Parameter of bridge pier	
Height of the pier	$L = 5.2\ m$
Mass density	$\rho_r = 2600\ kg/m^3$
Cross-section area	$A_c = 3.0772\ m^2$

Young's modulus of concrete	$E_c = 30.0\ GPa$
Reinforcement cross-section area	$A_y = 0.0157\ m^2$
Young's modulus of reinforcement	$E_y = 200\ GPa$

Table x. Properties of the girder and pier

Technical code in China requires considering equivalent parameters for design of highway reinforced concrete bridges. Hence, the equivalent section area of the girder $A = A_c + A_y(a_y - 1) + A_p(a_p - 1)$, the equivalent inertia moment of the girder is $I = I_c + I_y + I_p = 3.684\ m^4$, the equivalent flexural stiffness of the girder is $EI = 0.95E_cI = 1.21 \cdot 10^{11}\ Nm^2$. The equivalent Young's modulus of the of the pier is $E_r = (E_cA_c + E_yA_y)/(A_c + A_y) = 31.7\ GPa$, the equivalent section area of the pier *is* $A_r = A_c + A_y(a_y - 1)$ where $a_y = E_y/E_c$ is the enhancement coefficient. A circular plate rubber bearing, GYZ850 × 171, is installed between the girder and the pier. Recent theoretical and experimental studies on the vertical stiffness of rubber bearings indicate that the hysteresis curve of the rubber bearing is elongated and narrow, allowing the vertical stiffness to be considered constant. For simplicity in deriving a theoretical solution, this thesis treats the rubber bearing as an elastic spring, with its vertical stiffness estimated at *K = 2 × 10^9 N/m*.

The bridge is situated in a region with a seismic intensity of 8°. According to the Chinese seismic design code for buildings, the peak horizontal earthquake acceleration is 510 gal ($5.1\ m/s^2$). The peak vertical earthquake acceleration, as commonly recommended by engineering guidelines, is two-thirds of the horizontal value. However, studies have identified distinctive characteristics in the *V/H* response spectra Bozorgnia (2004). To accurately represent the vertical earthquake characteristics, the simplified *V/H* spectra used in reference Bozorgnia (2004) are adopted. The local site consists of firm soil, with source-to-site distances *(r_{seis})* of 3, 10, and 20 km, accordingly.

$$\lambda = \frac{V}{H} = \begin{cases} a & \text{for } T < 0.1s \\ a - \beta(T - 0.1) & \text{for } 0.1s \le T < 0.3s \\ 0.5 & \text{for } T \ge 0.3s \end{cases} \tag{2.64}$$

In this description, T represents the period of the vertical earthquake, α is the maximum ratio of vertical to horizontal ground motion *(V/H),* and β is the coefficient for linear attenuation. Specifically, *α = 1.5, β = 5*, and the critical time $t_{rc} =$ 0.5 s when the source-to-site distance *(r_{seis})* is 3 km; *α = 1.3, β = 4*, and $t_{rc} = 2.0\ s$ for a r_{seis} of 10 km; and α = 1.1, β = 3, and $t_{rc} =$ 4.0 s at 20 km r_{seis}. Seismic excitation often comprises a superposition of harmonic components derived via Fourier transformation. This thesis discusses two distinct linear elastic systems: the in-contact phase and the out-of-contact phase. The nonlinear interaction during seismic events, or pounding, is modeled in segments, alternating between these two states. Transitions between these systems are dictated by specific conditions for in-contact and out-of-contact states Eq.(2.1). Within each system, the equation of motion is solved using the superposition principle of linear harmonic motion. For simplification in theoretical analyses, simple harmonic motion substitutes for actual vertical seismic excitation. To capture the primary characteristic of the excitation, the peak acceleration of the simple harmonic motion is aligned with that of the actual vertical seismic excitation.

$$B_1(t) = B_1 \sin(\omega_1 t), \quad \omega_1 = \frac{2\pi}{T_1}, \quad B_1 = \frac{\lambda_1 a_H}{-\omega_1^2}$$
$$B_2(t) = B_2 \sin(\omega_2 (t - t_a)), \quad \omega_2 = \frac{2\pi}{T_2}, \quad B_2 = \frac{\lambda_2 a_H}{-\omega_2^2}, \quad t_a = \frac{x_0}{v} \tag{2.65}$$
$$B_3(t) = B_3 \sin(\omega_3 (t - t_b)), \quad \omega_3 = \frac{2\pi}{T_3}, \quad B_3 = \frac{\lambda_3 a_H}{-\omega_3^2}, \quad t_b = \frac{2x_0}{v}$$

In this context, *B1, B2,* and *B3* represent the peak displacements due to vertical seismic excitation, while ω_1, ω_2, *and* ω_3 correspond to the frequencies of these seismic excitations. Here, a_H denotes the peak acceleration of the horizontal seismic excitation, and v is the apparent wave velocity. It is important to note that, unless stated otherwise, the seismic excitation is assumed to be uniform throughout the subsequent numerical analysis.

3.2.2 Convergence of analysis outcome

To evaluate the convergence of the current method, a thorough numerical comparison of pounding force histories at various time-step increments is depicted in Fig.3.4. For increments of 0.1 s and 0.05 s, the outcomes display only smooth pounding forces lacking high-frequency oscillations. With increments of 0.02 s and 0.01 s, high-frequency oscillations are present, but the accuracy of contact time, separation time, and pounding force is compromised. The time histories for the time increment of 0.001 seconds, the analysis yields precise and accurate results for the pounding force. Consequently, this time step has been selected for further analysis. Additionally, using a smaller time step would require significantly more computational resources, thus affirming the efficiency and efficacy of the chosen increment. Nonetheless, capturing transient wave phenomena such as shear force waves, bending moment waves in the girder, and axial force waves in the pier requires even smaller time-step increments. For instance, considering the longitudinal wave velocity in a St. Venant rod, which is 3492 m/s, the maximum time-step increment should be less than the time it takes for the wave to travel the length of the pier, approximately 1.5e-3 s. To accurately observe the axial force wave propagation, smaller increments are necessary, leading to the use of 1.0e-5 s increments in this analysis to effectively capture the transient wave propagation, including that induced by pounding.

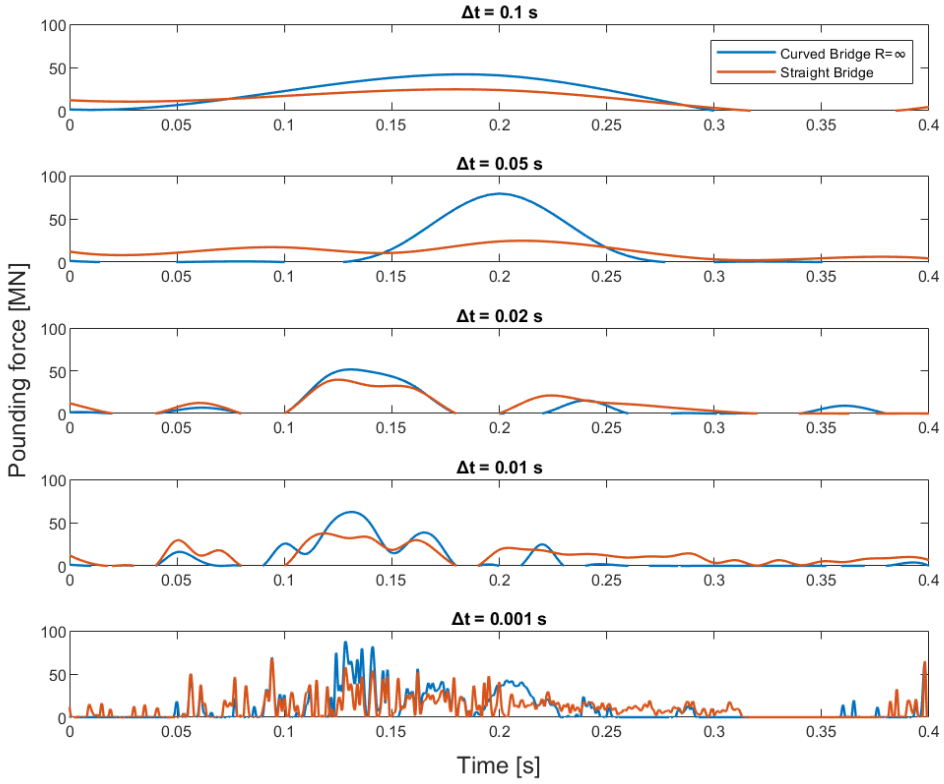

Fig. 3.4. Pounding force generated in curved bridge (R=∞) vs straight bridge computed by different time increment ($N = 25, \lambda = 0.5$ and $T = 0.3\ s$)

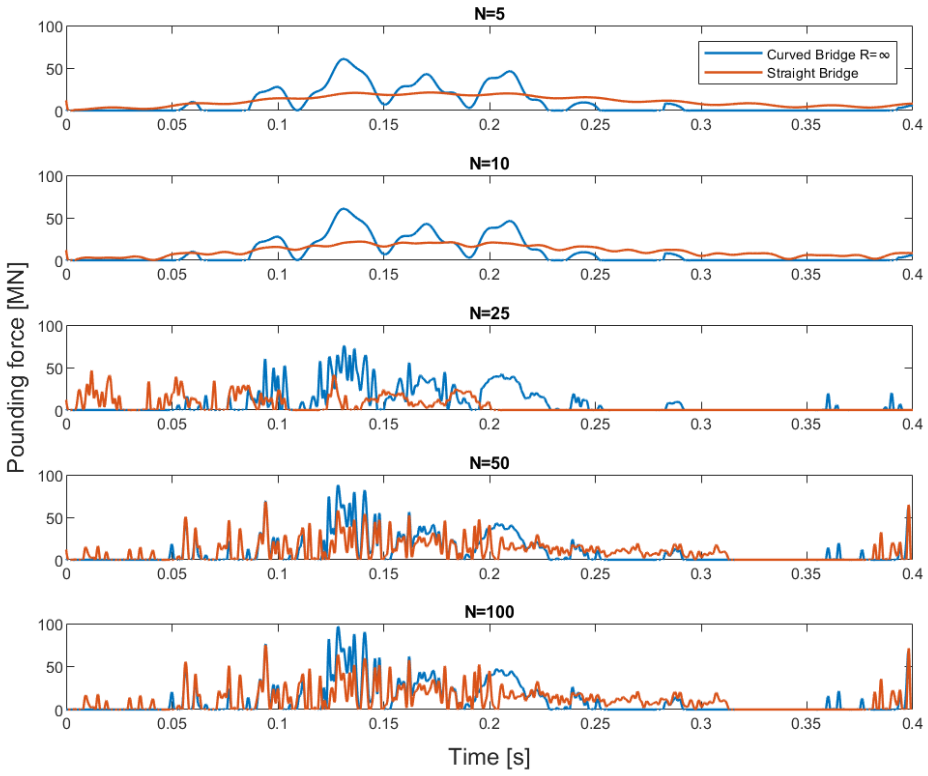

Fig. 3.5. Pounding force generated in curved bridge (R=∞) vs straight bridge computed by different number of modes ($\Delta t = 0.001$ s, $\lambda = 0.5$ and $T = 0.3\ s$)

Additionally, the convergence related to the number of wave modes is assessed by analyzing the time histories of pounding force for truncation term numbers of 5, 10, 25, 50 and 100 as shown in Fig.x. With a truncation number of 5, the pounding force history appears smooth, losing significant high-frequency detail. Increasing the number to 10 introduces some high-frequency elements. However, with 25, the measures of contact time, separation time, and pounding force remain imprecise. The histories for wave mode numbers of 50 and 100 are closely aligned, demonstrating convergence in the time history of multiple-pounding forces. To address high-frequency transient responses adequately, larger wave modes are essential.

3.2.3 Wave propagation across the beam induced by vertical ground motion

Fig-x illustrates the propagation of structural response waves induced by a vertical earthquake, displaying the travel of shearing force and bending moment waves across the structure. The horizontal axes s is normalized by s_0. Fig.3.6 depicts the movement of the shearing force wave along the girder following the onset of the vertical earthquake, with waveforms at moments $t = 0.1\ ms$, $0.5\ ms$, and $1.0\ ms$. These waves fluctuate around the static shearing force and visibly progress from the ends towards the center of the girder, disturbing the static shearing force as they arrive.

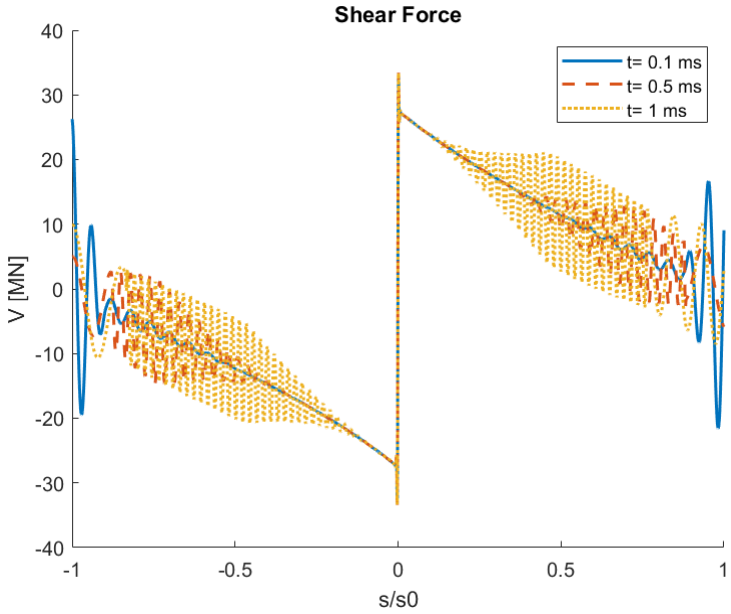

Fig. 3.6. Shearing forve wave propagation along the girder of curved bridge with R=70 m ($N = 25$, $\Delta t = 0.001$ s, $\lambda = 0.5$ and $T = 0.3\ s$)

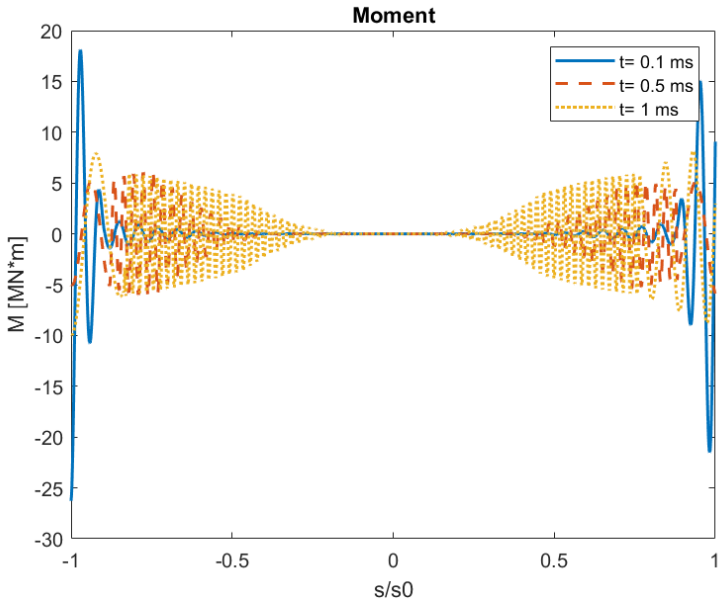

Fig. 3.7. Dynamic bending moment wave propagation along the girder of curved bridge with R=70 m ($N = 25$, $\Delta t = 0.001$ s, $\lambda = 0.5$ and $T = 0.3$ s)

Fig.3.7 presents the propagation of the dynamic bending moment wave along the girder. The waveforms at the same instants show that the dynamic bending moment, which is the difference between the total and static bending moments, also advances from both ends towards the middle. Wave propagation along the girder exhibits dispersive characteristics. In addition, obtained data indicate that the two ends of the girder experience more dynamic excitation compared to the mid-span of the girder. Such increased activity at the ends highlights the significant impact of seismic forces initiating from these points and emphasizes the need for careful consideration of end conditions in structural design and analysis.

3.2.4 Multiple pounding phenomena

This section provides detailed information about the effects of curvature on the pounding force. As it was mentioned before, the chord length will be kept constant while the beam gets more curved till to the almost half-ring shape, though the last one is not applicable in real engineering practice.

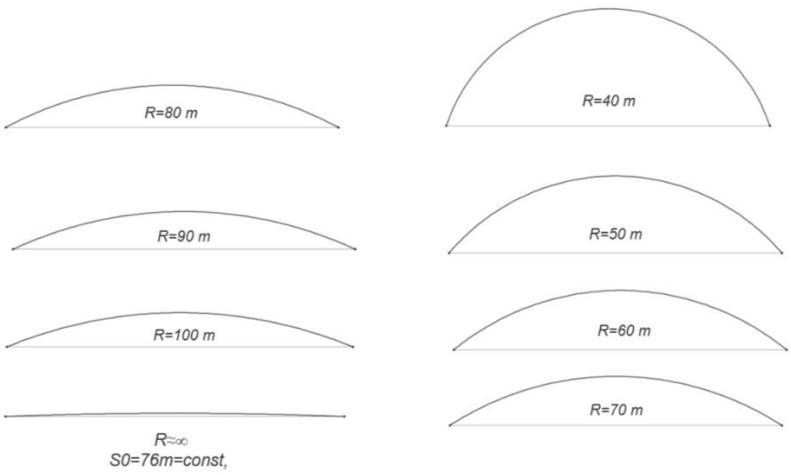

Fig 3.8. Comparative diagrams of bridge curvatures

The Fig.3.9 (from a-g) shows a distinct pattern where the magnitude and the frequency of the contact force vary with the radius. Generally, with the increasing the radius, the behavior of pounding forces seems to stabilize and become less intense. On the other hand, for smaller radii (eg., R=40÷60 m), the pattern is more erratic and exhibit higher peak values. It means that tighter curvatures may lead to more significant interactions or collisions between girder and pier due to the more pronounced movement or deflections in more curved bridges. Moreover, as radius decreases, the span length of a bride increases, leading to an increase of the self-weight of girder, meaning that contact force will be higher due to altered static conditions. This will cause the concentration of forces at specific points, particularly where the girder meets the columns.

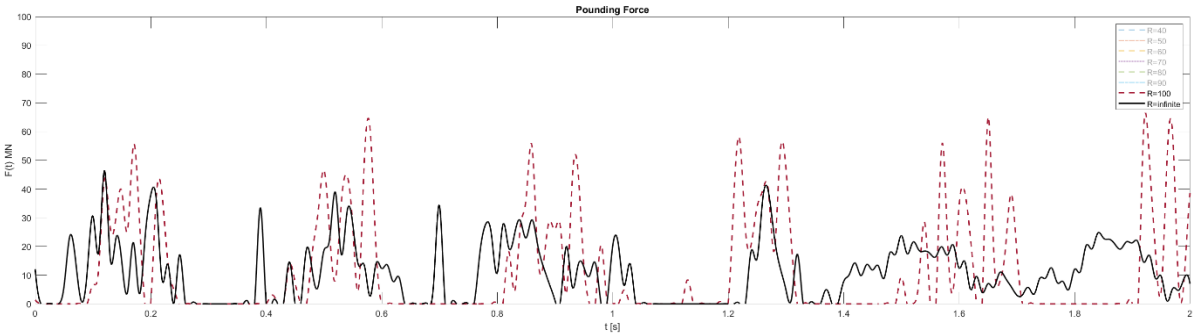

(a)

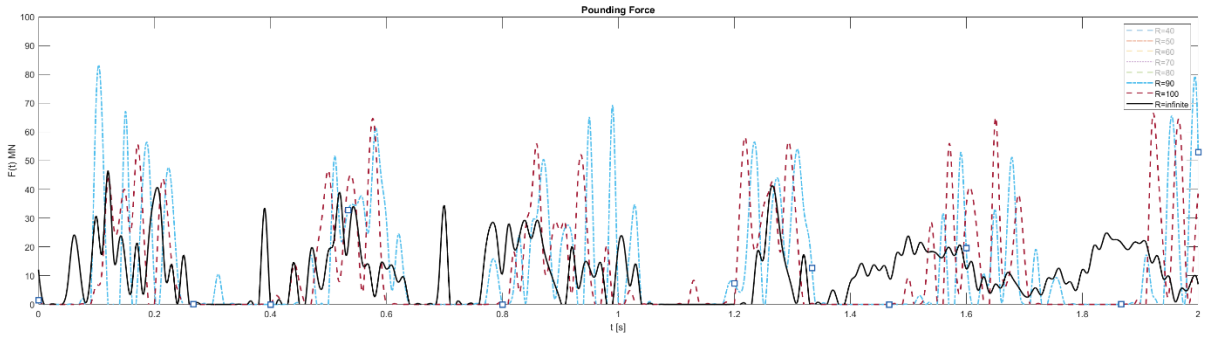

(b)

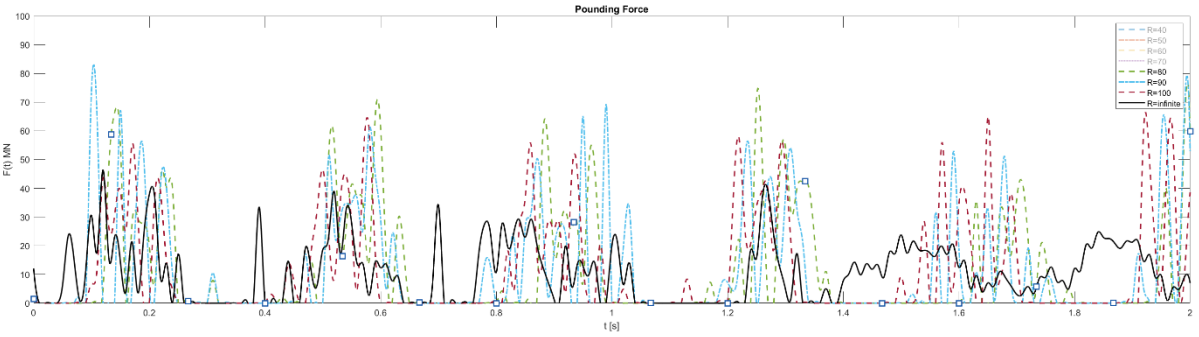

(c)

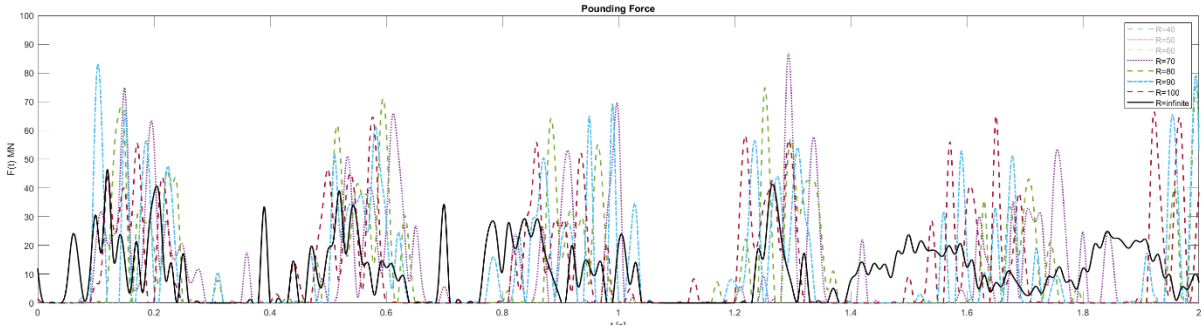

(d)

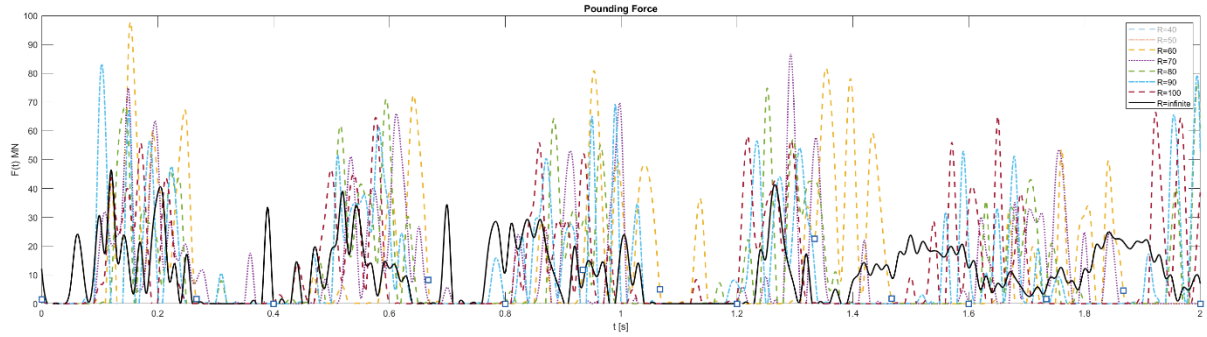

(e)

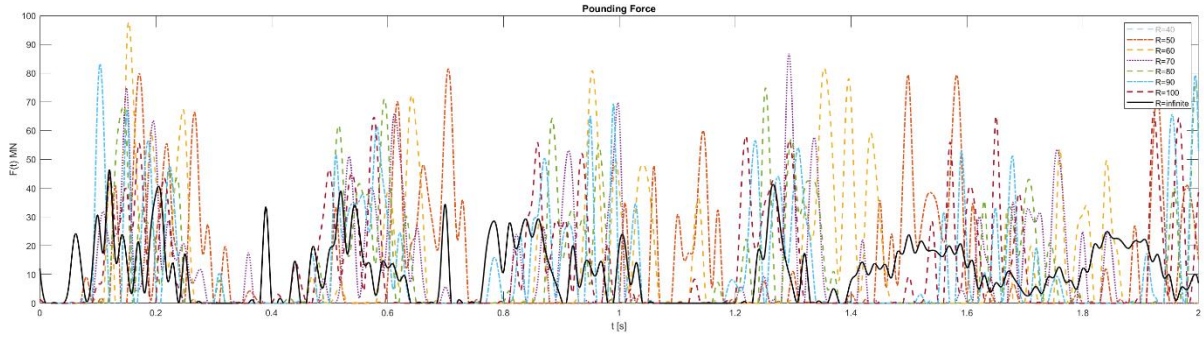

(f)

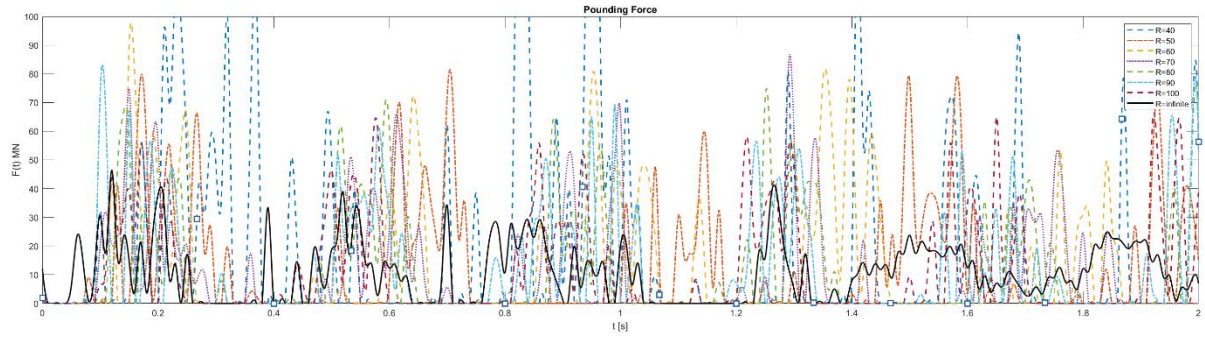

(g)

Fig 3.9. The effect of the curvature (R=40÷∞) on pounding force dynamics ($N = 25$, $\Delta t = 0.001$ s, $\lambda = 0.5$ and $T = 0.3$ s)

It is worth to note that, in addition to above listed observations, the curved geometry may cause asymmetrical load transfer during the seismic event, where the different sides might experience

different level of stress. Another remarkable fact is that the angular component of the earthquake seismic waves could cause more pronounced rotational and lateral movement of the bridge girder relative the pier which might cause the increase of the frequency and intensity of collisions between bridge segments. Seismic waves typically travel in all directions from their sources, but when they encounter structures, they path can be altered based on the layout and properties of the material of a structure. In straight, uniform structures, seismic waves might propagate more predictably which can't be said about curved paths. From design perspective, engineers need to account for these amplified forces by incorporating additional damping or isolation system, especially at critical junctions

To better understand the trend of the pounding force under different radius of curvature, it is advisable to plot the peak and mean pounding forces versus the radius and curvature of the bridge (see Fig.3.10.a). In first graph, it shows clear increase in both mean and maximum pounding forces as the curvature increases. This can be attributed to the elongated span which weighs more than less curved girders. As regards the Fig.3.10.b, the pounding force shows non-linear behavior. Both the maximum and mean forces decrease from $R = 40\,m$ to $R = 70\,m$, then slightly increase at $R = 80\,m$ before dropping again. It suggests that wider curves moderate the impact of seismic forces, however, slightly increase at $R = 80\,m$ may indicate specific structural responses that could be unique to certain bridge geometries. Nevertheless, the analysis was conducted with time interval 2 s, and the output could be more accurate and reliable under longer period of time.

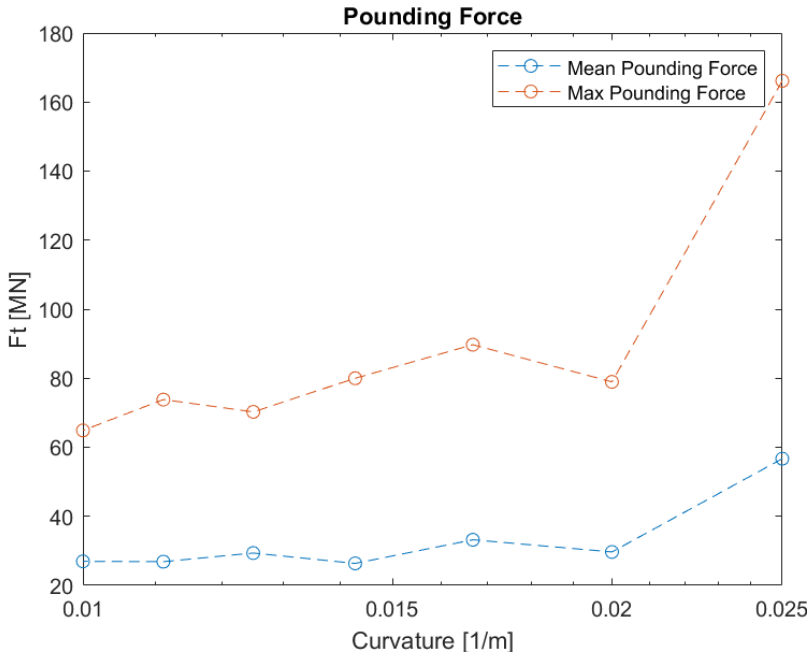

(a)

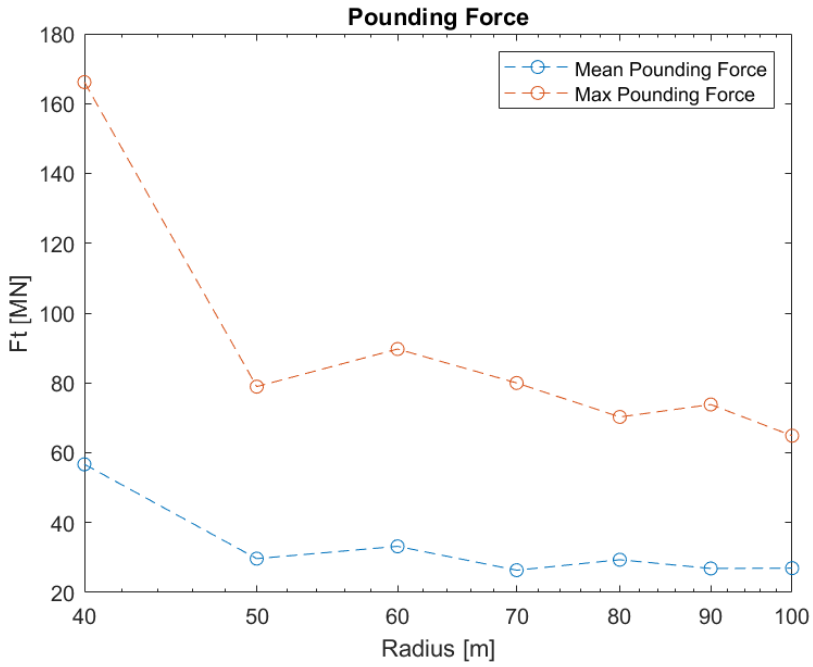

(b)

Fig 3.10. The impact of the curvature (a) and the radius (b) on pounding force vibration ($N = 25$, $\Delta t = 0.001$ s, $\lambda = 0.5$ and $T = 0.3$ s)

3.2.5 Mode shapes

Below graphs provides information about mode shapes of the curved bridge ($R = 70\,m$) both in-contact and out-of-contact phases. Each mode shape represents the deformation pattern of the structure under seismic excitation with different characteristics observed based on phase and mode number. When the girder is in contact with the pier, it demonstrates the figure possibly involving sections where the beam and rod mechanically engaged due to vertical ground motion. Note that mode shapes are always symmetrical indicating both beam and rod vibrates with the same frequency. On contrary, the mode shapes are more uniformly distributed and smoother in separation phase pointing out less constrained deformation. The figure in this case shows symmetrical shapes for odd numbers of N and asymmetrical for even numbers of N. However, for both cases, mode shapes are more complex behavior as the number of modes increases.

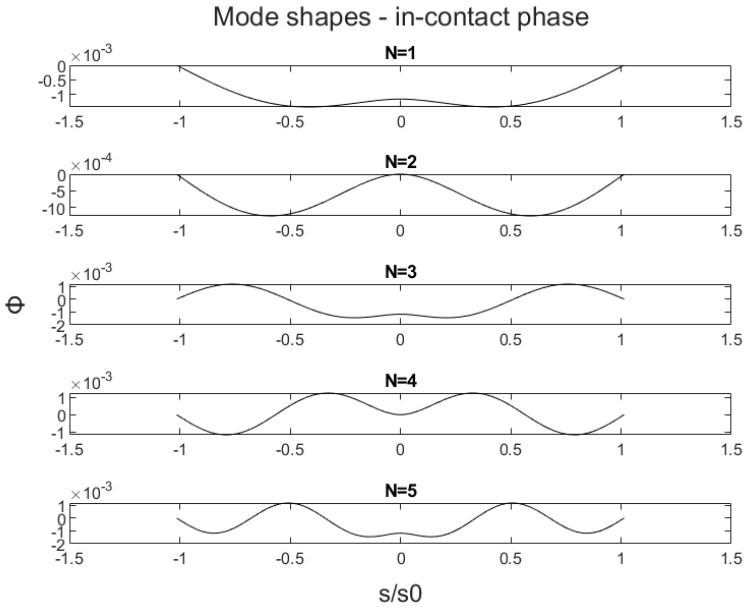

(a)

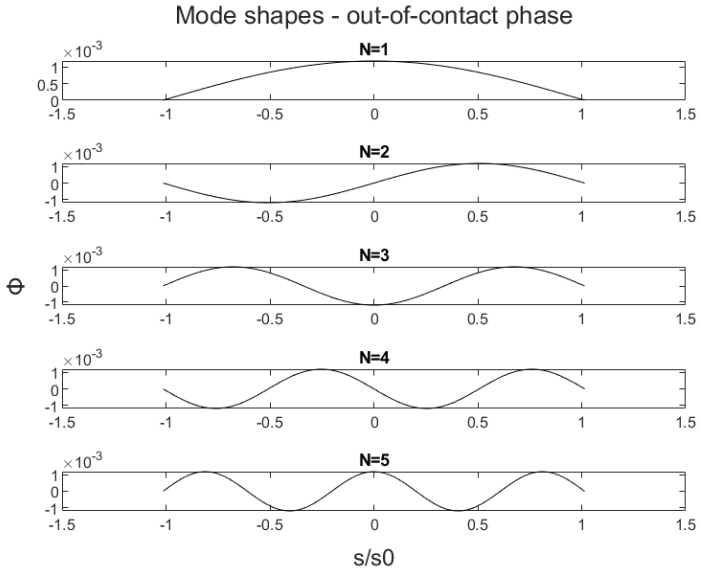

(b)

Fig 3.11. Mode shapes for in-contact phase (a) and out-of-contact phase (b)

3.2.6 Response of the bridge under uniform seismic excitation

The bridge's natural periods were determined analytically and validated by Finite Element Modeling (FEM) using SAP2000. The natural period in the separation phase is 0.176 seconds and 0.062 seconds in the in-contact phase, with FEM adjustments showing a slight increase for the in-contact phase to 0.082 seconds.

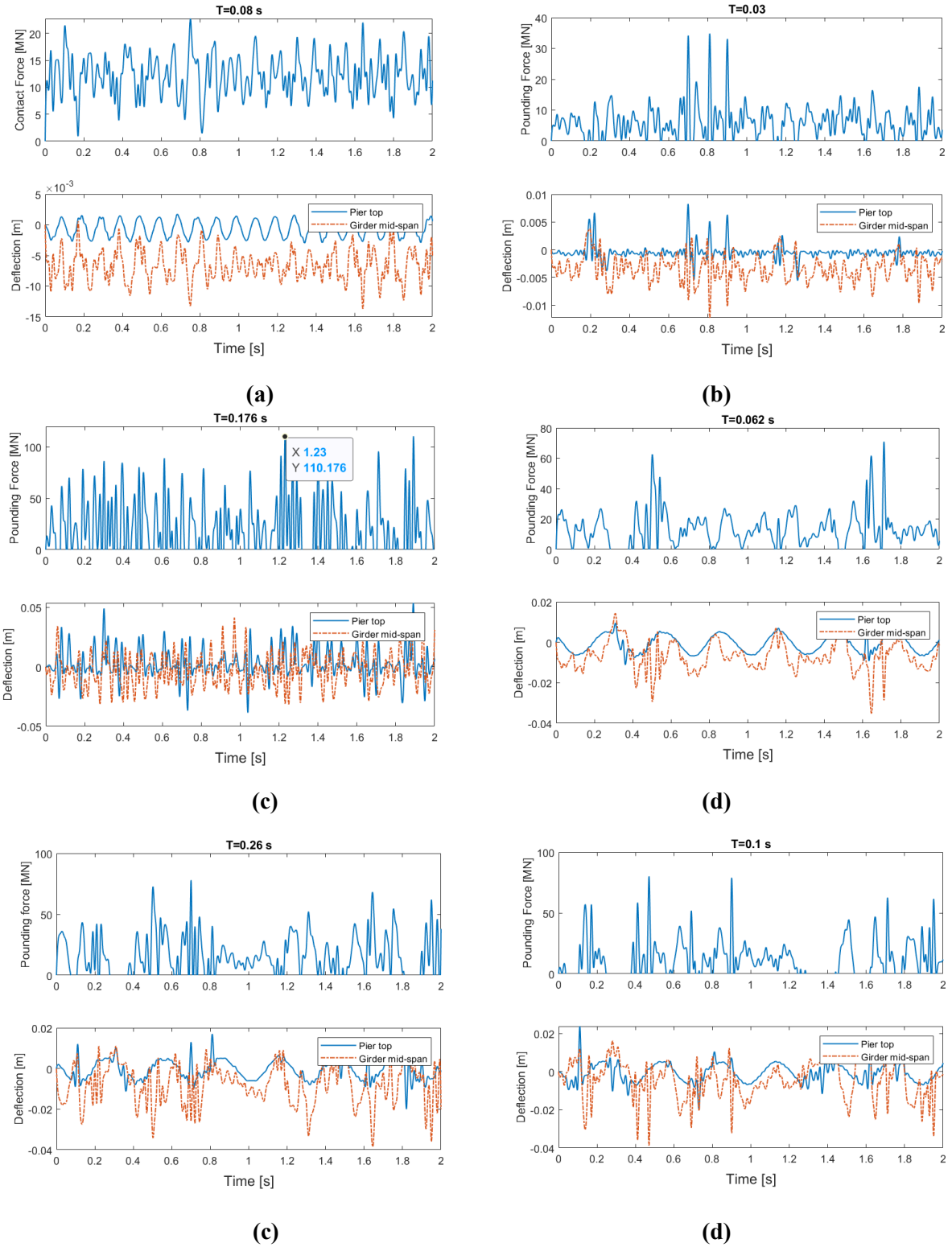

Fig 3.12. Responses of the bridge in different vertical seismic excitation periods

When the bridge was excited at its natural period during the separation phase, the maximum pounding force was observed as 110.2 MN with 15 multiple poundings, and the frequency of pounding incidents was significantly higher compared to other tested periods. On the other hand, when the bridge was excited by T=0.08 s, it resulted minimal or no multiple pounding events, indicating that reducing the period to half of the natural frequency significantly reduces the intensity and frequency of interactions

between the bridge components. Increased by half natural period T=0.26 s showed reduced pounding compared to the natural period but still resulted in a notable number of pounding incidents (10 times).

The findings clearly demonstrate that aligning the seismic excitation period with the bridge's natural period, especially during the separation phase, dramatically increases both the peak pounding force and the number of pounding events. This suggests that resonance effects are significant and potentially damaging under these conditions.

Conclusion

This thesis has provided an in-depth analysis of the seismic responses of horizontally curved bridges, with a specific emphasis on the phenomenon of pounding effects, which are critical to the structural integrity of these constructions during earthquakes. Building upon the foundational work of X. Yin (2015), this research adapted and extended existing models to better understand and predict the dynamic interactions specific to curved bridge geometries under seismic loads.

One of the key aspect of this study was the detailed analysis of how the number of modes and time steps affect the convergence of results in the computational models. By gradually varying these parameters, the research demonstrated that both factors play crucial roles in achieving accurate and stable simulation outcomes. The appropriate selection of mode numbers and time increments was shown to critically influence the precision of the modeled seismic responses, ensuring reliable predictions of the dynamic behaviors observed in curved bridges.

Furthermore, the thesis explored wave propagation phenomena along the bridge structure, providing novel insights into how seismic waves are transmitted through curved bridge geometries. It was observed that the dynamic waves initially impact the ends of the bridge before progressively moving toward the center which means under the higher vertical ground motions, ends of the girder experiences higher dynamic load. This propagation pattern underscores the importance of considering the spatial distribution of dynamic effects when designing bridges to withstand seismic forces.

The research has shown that seismic period matching, where the seismic excitations align with the bridge's natural periods, significantly exacerbates the pounding effects. This alignment typically leads to increased forces and stresses at the girder-pier interfaces, highlighting potential vulnerabilities in bridge design. By varying the seismic periods around the bridge's natural frequencies—both in-contact and out-of-contact phases—we observed noticeable differences in how these forces manifest, providing crucial insights into effective seismic design strategies.

Specifically, the simulations indicated that when the excitation periods are slightly shorter or longer than the natural periods, the severity of pounding forces can be mitigated. This suggests that avoiding resonance phenomena through careful tuning of structural frequencies could be a key strategy in reducing the risk of damage during earthquakes.

The outcomes of this thesis not only advance our understanding of how horizontally curved bridges respond to seismic forces but also serve as a critical resource for engineers and designers. The insights gained from this research should inform future designs, promoting the integration of seismic resilience features that can accommodate and counteract the dynamic challenges posed by bridge curvature. It is recommended that future studies continue to explore innovative materials and dynamic damping solutions that can further enhance the resilience of curved bridges to seismic activities.

In conclusion, this thesis underscores the necessity for targeted seismic design considerations in the development of curved bridges, ensuring their safety and functionality in the face of seismic challenges. The strategic incorporation of the findings from this research into engineering practices can lead to the construction of safer, more durable structures in seismically active regions.

Appendix:

1. In order to find solution for $\frac{d^2M}{d\varphi^2} + M = -q \cdot r^2$, let's look for solution in the form of $M(\varphi) = e^{m\varphi}$ and substituting into above equation we obtain:

$$\frac{d^2(e^{m\varphi})}{d\varphi^2} + e^{m\varphi} = 0$$

$$\frac{d^2(e^{m\varphi})}{d\varphi^2} + e^{m\varphi} = 0$$

$$\left(m^2 + 1\right)e^{m\varphi} = 0 \rightarrow m = \pm i$$

$$M(\varphi) = Ae^{i\varphi} + Be^{-i\varphi}$$

Since we know that $e^{i\varphi} = \cos\varphi + i\sin\varphi$ and $e^{-i\varphi} = \cos\varphi - i\sin\varphi$,the homogenous solution can rewritten as:

$$M(\varphi) = A\cos\varphi + A\sin\varphi + B\cos\varphi - B\sin\varphi$$

$$C_1 = A + B\,, C_2 = A - B$$

$$M(\varphi)_h = C_1\cos\varphi + C_2\sin\varphi$$

Particular solution takes the form:

$$M(\varphi)_p = -qR^2$$

Finally, we get:

$$M(\varphi) = C_1\cos\varphi + C_2\sin\varphi - qR^2$$

1. To demonstrate orthogonality condition, let's consider two modes called ϕ_n and ϕ_m:

$$EI\frac{\partial^4\phi_{bn}}{\partial s^4} = \omega_n^2\rho A\phi_{bn}$$

$$EI\frac{\partial^4\phi_{bm}}{\partial s^4} = \omega_n^2\rho A\phi_{bm}$$

Multiplying both modes to each other and taking integration both sides along the length of the beam:

$$EI\int\frac{\partial^4\phi_{bn}(s)}{\partial s^4}\phi_{bm}(s)ds = \omega_n^2\int\rho A\phi_{bn}(s)\phi_{bm}(s)ds$$

$$EI\int\frac{\partial^4\phi_{bm}(s)}{\partial s^4}\phi_{bn}(s)ds = \omega_n^2\int\rho A\phi_{bm}(s)\phi_{bn}(s)ds$$

Performing the same operation for rod and second half of the beam and subtracting obtained equation, one gets:

$$\left(\omega_n^2-\omega_m^2\right)\left[\int_{-s_0}^{0}\rho A\phi_{bn1}(s)\phi_{bm1}(s)ds+\int_{0}^{s_0}\rho A\phi_{bn2}(s)\phi_{bm2}(s)ds+\int_{0}^{L}\rho_r A_r\phi_{rn}(\xi)\phi_{rm}(\xi)ds\right]=\begin{Bmatrix}0\\1\end{Bmatrix}$$

Above expression is equal to Dirac function and when $m \neq n$ is zero and when $m = n$ becomes 1.

2. After applying boundary condition provided in Eq.(2.44), the set of equations are formed:

$$\begin{cases}
-EIk_b^3A_{n1}+EIk_b^3C_{n1}-EIk_b^3A_{n2}+EIk_b^3C_{n2}-k_rT_nE_rA_r\cos k_r=0\\
-A_{n1}\sin k_bs_0+B_{n1}\cos k_bs_0-C_{n1}\sinh k_bs_0+D_{n1}\cosh k_bs_0=0\\
A_{n2}\sin k_bs_0+B_{n2}\cos k_bs_0+C_{n2}\sinh k_bs_0+D_{n2}\cosh k_bs_0=0\\
k_b^2A_{n1}\sin k_bs_0-k_b^2B_{n1}\cos k_bs_0-k_b^2C_{n1}\sinh k_bs_0+k_b^2D_{n1}\cosh k_bs_0=0\\
-k_b^2A_{n2}\sin k_bs_0-k_b^2B_{n2}\cos k_bs_0+k_b^2C_{n2}\sinh k_bs_0+k_b^2D_{n2}\cosh k_bs_0=0\\
B_{n1}+D_{n1}=B_{n2}+D_{n2}\\
A_{n1}+C_{n1}=A_{n2}+C_{n2}\\
-B_{n1}+D_{n1}=-B_{n2}+D_{n2}\\
-B_{n1}+D_{n1}-E_n\left(\sin k_rL+E_rA_rk_r\cos k_rL/K\right)=0\\
F_n=0
\end{cases}$$

Once system of equations is identified, beam coefficients can be now determined:

$$A_{n1}=-\frac{\cos k_bs_0\cosh k_bs_0E_n\left(\dfrac{E_rA_rk_r\cos k_rL}{K}+\sin k_rL\right)}{\cos k_bs_0\sinh k_bs_0-\sin k_bs_0\cosh k_bs_0}$$

$$B_{n1}=\frac{\sin k_bs_0\cosh k_bs_0E_n\left(\dfrac{E_rA_rk_r\cos k_rL}{K}+\sin k_rL\right)}{\sin k_bs_0\cosh k_bs_0-\cos k_bs_0\sinh k_bs_0}$$

$$C_{n1}=-\frac{\cos k_bs_0\cosh k_bs_0E_n\left(\dfrac{E_rA_rk_r\cos k_rL}{K}+\sin k_rL\right)}{\sin k_bs_0\cosh k_bs_0-\cos k_bs_0\sinh k_bs_0}$$

$$D_{n1}=-\frac{\cos k_bs_0\sinh k_bs_0E_n\left(\dfrac{E_rA_rk_r\cos k_rL}{K}+\sin k_rL\right)}{\sin k_bs_0\cosh k_bs_0-\cos k_bs_0\sinh k_bs_0}$$

$$A_{n2}=\frac{\cos k_bs_0\cosh k_bs_0E_n\left(\dfrac{E_rA_rk_r\cos k_rL}{K}+\sin k_rL\right)}{\cos k_bs_0\sinh k_bs_0-\sin k_bs_0\cosh k_bs_0}$$

$$B_{n2} = \frac{\sin k_b s_0 \cosh k_b s_0 E_n \left(\dfrac{E_r A_r k_r \cos k_r L}{K} + \sin k_r L \right)}{\sin k_b s_0 \cosh k_b s_0 - \cos k_b s_0 \sinh k_b s_0}$$

$$C_{n2} = \frac{\cos k_b s_0 \cosh k_b s_0 E_n \left(\dfrac{E_r A_r k_r \cos k_r L}{K} + \sin k_r L \right)}{\sin k_b s_0 \cosh k_b s_0 - \cos k_b s_0 \sinh k_b s_0}$$

$$D_{n2} = -\frac{\cos k_b s_0 \sinh k_b s_0 E_n \left(\dfrac{E_r A_r k_r \cos k_r L}{K} + \sin k_r L \right)}{\sin k_b s_0 \cosh k_b s_0 - \cos k_b s_0 \sinh k_b s_0}$$

Substituting all these coefficients into orthogonality condition, it is possible to determine undefined coefficient E_n:

$$E_n^{-2} = M_n \left(\int_{-s_0}^{0} \rho A \left[-\frac{\sin k_b (s+s_0)}{\cos k_b s_0} + \frac{\sinh k_b (s+s_0)}{\cosh k_b s_0} \right]^2 ds + \int_{0}^{s_0} \rho A \left[\frac{\sin k_b (s-s_0)}{\cos k_b s_0} - \frac{\sinh k_b (s-s_0)}{\cosh k_b s_0} \right]^2 ds \right)$$

$$+ \int_0^L \rho_r A_r \sin^2 k_r \xi d\xi = M_n^2 \rho A s_0 \left(\frac{\sin^2 k_b s_0}{\cos^2 k_b s_0} + \frac{\sinh^2 k_b s_0}{\cosh^2 k_b s_0} \right) + \frac{\rho_r A_r}{8 k_r} \sin 2 k_r L + \frac{3 \rho_r A_r E_r^2 \cos^2 k_r L}{4K} + \rho_r A_r \frac{L}{2}$$

Where M_n is the coefficient related beam-rod frequency equation:

$$M_n = \frac{E_r A_r k_{nr} \cos k_{nr} L}{4 E I k_{bn}^3} = \frac{\sin k_{nr} L + \dfrac{E_r A_r k_{rn} \cos k_{rn} L}{K}}{\tanh k_{bn} s_0 - \tan k_{bn} s_0}$$

Sources:

Abu-Hilal, M. 'Forced Vibration of Euler–Bernoulli Beams by Means of Dynamic Green Functions'. *Journal of Sound and Vibration*, vol. 267, no. 2, Oct. 2003, pp. 191–207. *DOI.org (Crossref)*, https://doi.org/10.1016/S0022-460X(03)00178-0.

Agarwal, Preeti, et al. 'Finite Element Analysis of Reinforced Concrete Curved Box-Girder Bridges'. *Advances in Bridge Engineering*, vol. 4, no. 1, Feb. 2023, p. 1. *DOI.org (Crossref)*, https://doi.org/10.1186/s43251-023-00080-7.

Amjadian, Mohsen, and Anil K. Agrawal. 'Rigid-Body Motion of Horizontally Curved Bridges Subjected to Earthquake-Induced Pounding'. *Journal of Bridge Engineering*, vol. 21, no. 12, Dec. 2016, p. 04016090. *DOI.org (Crossref)*, https://doi.org/10.1061/(ASCE)BE.1943-5592.0000962.

Bozorgnia, Yousef, and Kenneth W. Campbell. 'The Vertical-to-Horizontal Response Spectral Ratio and Tentative Procedures for Developing Simplified v/h and Vertical Design Spectra'. *Journal of Earthquake Engineering*, vol. 08, no. 02, Mar. 2004, pp. 175–207. *worldscientific.com (Atypon)*, https://doi.org/10.1142/S1363246904001481.

Chai Hong Yoo. 'A Consistent Discrete Elements Technique for Curved Members'. *Computers & Structures*, vol. 25, no. 1, Jan. 1987, pp. 137–46. *DOI.org (Crossref)*, https://doi.org/10.1016/0045-7949(87)90225-2.

Culver, Charles G. 'Natural Frequencies of Horizontally Curved Beams'. *Journal of the Structural Division*, vol. 93, no. 2, Apr. 1967, pp. 189–204. *ASCE*, https://doi.org/10.1061/JSDEAG.0001641.

Earthq Engng Struct Dyn - 2015 - Yang - Transient Responses of Girder Bridges with Vertical Poundings under Near-fault.Pdf.

Gere, James M. *Mechanics of Materials, Brief Ed.* 2011.

Gupta, Tanmay, and Dikshit Sandhu. 'Seismic Response of Horizontally Curved Bridges in Combination with Skewed Abutments'. *Structures*, vol. 36, Feb. 2022, pp. 864–78. *DOI.org (Crossref)*, https://doi.org/10.1016/j.istruc.2021.12.068.

Howson, W. P., et al. 'Exact Natural Frequencies for Out-of-Plane Motion of Plane Structures Composed of Curved Beam Members'. *Computers & Structures*, vol. 55, no. 6, June 1995, pp. 989–95. *DOI.org (Crossref)*, https://doi.org/10.1016/0045-7949(94)00524-7.

Irie, T., et al. 'Natural Frequencies of Out-of-Plane Vibration of Arcs'. *Journal of Applied Mechanics*, vol. 49, no. 4, Dec. 1982, pp. 910–13. *DOI.org (Crossref)*, https://doi.org/10.1115/1.3162635.

Irie, Toshihiro, et al. *Various Types of Out-of-Plane Vibration of Arcs*.

Jennings, Paul, and John Wood. 'Engineering Features of the San Fernando Earthquake'. *Bulletin of the New Zealand Society for Earthquake Engineering*, vol. 6, Mar. 1973, pp. 22–45. *ResearchGate*, https://doi.org/10.5459/bnzsee.6.1.22-45.

Kang, Kijun, et al. 'Vibration Analysis of Horizontally Curved Beams with Warping Using DQM'. *Journal of Structural Engineering*, vol. 122, no. 6, June 1996, pp. 657–62. *DOI.org (Crossref)*, https://doi.org/10.1061/(ASCE)0733-9445(1996)122:6(657).

Klikowicz, Piotr, et al. *Specific Problems of Bridges with Big Curvature in Plan*. 2013. *DOI.org (Datacite)*, https://doi.org/10.13140/2.1.4307.4568.

Komatsu, Sadao, and Hiroshi Nakai. 'STUDY ON FREE VIBRATION OF CURVED GIRDER BRIDGES'. *Transactions of the Japan Society of Civil Engineers*, vol. 1966, no. 136, 1966, pp. 35–60. *DOI.org (Crossref)*, https://doi.org/10.2208/jscej1949.1966.136_35.

Li, Nana, et al. 'Experimental Research on Adjacent Pounding Effect of Midspan Curved Bridge with Longitudinal Slope'. *Engineering Structures*, vol. 196, Oct. 2019, p. 109320. *DOI.org (Crossref)*, https://doi.org/10.1016/j.engstruct.2019.109320.

Mairone, Mattia, et al. 'Behaviour and Analysis of Horizontally Curved Steel Box-Girder Bridges'. *Open Journal of Civil Engineering*, vol. 12, no. 03, 2022, pp. 390–414. *DOI.org (Crossref)*, https://doi.org/10.4236/ojce.2022.123022.

Pang, Chen. *] CURVED BRIDGE SUBJECTED TO SIM ULATED I HIGHW AY LOADINGS.*

Reis, António J., and José J. Oliveira Pedro. *Bridge Design: Concepts and Analysis*. 1st ed., Wiley, 2019. *DOI.org (Crossref)*, https://doi.org/10.1002/9781118927595.

Suzuki, Katsuyoshi, and Shin Takahashi. 'Out-Plane Vibrations of Curved Bars Considering Shear Deformation and Rotatory Inertia'. *Bulletin of JSME*, vol. 24, no. 193, 1981, pp. 1206–13. *J-Stage*, https://doi.org/10.1299/jsme1958.24.1206.

Xiaochun Yin. 'Transient Responses of Girder Bridges with Vertical Poundings under Near-Fault Vertical Earthquake'. *Earthquake Engng Struct. Dyn. 2015*, vol. 44, no. 15, Dec. 2015, pp. 2637–57. *Wiley Online Library*, https://doi.org/10.1002/eqe.2601.